AWARD NUMBER: W81XWH-12-1-0164

TITLE: Comparative Oncogenomics for Peripheral Nerve Sheath Cancer Gene Discovery

PRINCIPAL INVESTIGATOR: Steven L. Carroll, MD, PhD

RECIPIENT: Medical University of South Carolina
Charleston, SC 29425

REPORT DATE: June 2015

TYPE OF REPORT: Annual

PREPARED FOR: U.S. Army Medical Research and Materiel Command
Fort Detrick, Maryland 21702-5012

REPORT DOCUMENTATION PAGE

Form Approved
OMB No. 0704-0188

1. REPORT DATE	2. REPORT TYPE	3. DATES COVERED
June 2015	Annual	1Jun2014 - 31May2015

4. TITLE AND SUBTITLE

Comparative Oncogenomics for Peripheral Nerve Sheath Cancer Gene Discovery

5a. CONTRACT NUMBER
W81XWH-12-1-0164

5b. GRANT NUMBER

5c. PROGRAM ELEMENT NUMBER

6. AUTHOR(S)

Steven L. Carroll

E-Mail: carrolst@musc.edu

5d. PROJECT NUMBER

5e. TASK NUMBER

5f. WORK UNIT NUMBER

7. PERFORMING ORGANIZATION NAME(S) AND ADDRESS(ES)
Medical University of South Carolina
Charleston, SC 29425

8. PERFORMING ORGANIZATION REPORT NUMBER

9. SPONSORING / MONITORING AGENCY NAME(S) AND ADDRESS(ES)

U.S. Army Medical Research and Materiel Command
Fort Detrick, Maryland 21702-5012

10. SPONSOR/MONITOR'S ACRONYM(S)

11. SPONSOR/MONITOR'S REPORT NUMBER(S)

12. DISTRIBUTION / AVAILABILITY STATEMENT

Approved for Public Release; Distribution Unlimited

13. SUPPLEMENTARY NOTES

14. ABSTRACT

We have developed a robust transgenic mouse model (P0-GGFβ3 mice) in which overexpression of the growth factor neuregulin-1 (NRG1) results in the reproducible development of plexiform neurofibromas which subsequently progress to become MPNSTs. We hypothesized that comprehensively characterizing alterations in the genomes and gene expression profiles of peripheral nerve sheath tumors arising in our P0-GGFβ3 mouse model will identify candidate driver genes mediating plexiform neurofibroma pathogenesis and neurofibroma-MPNST progression, thereby identifying new therapeutic targets in the equivalent human tumors. To test this overarching hypothesis, we are using a comprehensive multi-tiered process to identify candidate driver mutations in P0-GGFβ3 neurofibromas and MPNSTs, establish gene signatures defining distinct tumor subtypes and functionally test the role of selected driver mutations characteristic of specific subtypes. Potential driver mutations within relatively large regions of chromosomal gain or loss will be identified using high density array comparative genomic hybridization (aCGH) and cross-species comparisons of this data with aCGH findings from human neurofibromas and MPNSTs. Smaller mutations (missense mutations, nonsense mutations, small indels and fusion events) will be identified using a combination of transcriptome (RNA-Seq) and exome sequencing in these same murine tumors. The contribution of selected candidate driver mutations characteristic of specific tumor subtypes will be validated by manipulating the function of these genes and examining the effect this has in vivo, using orthotopically allografted tumor cells, and a variety of in vitro functional assays. We will validate the relevance of these mutated mouse genes in human neurofibromas and MPNSTs by determining whether these same genes are mutated in human tumors.

15. SUBJECT TERMS
Nothing listed

16. SECURITY CLASSIFICATION OF:			17. LIMITATION OF ABSTRACT	18. NUMBER OF PAGES	19a. NAME OF RESPONSIBLE PERSON
a. REPORT	b. ABSTRACT	c. THIS PAGE			USAMRMC
Unclassified	Unclassified	Unclassified	Unclassified	29	19b. TELEPHONE NUMBER *(include area code)*

Table of Contents

INTRODUCTION

We have developed a robust transgenic mouse model (P_0-GGFβ3 mice) in which overexpression of the growth factor neuregulin-1 (NRG1) results in the reproducible development of plexiform neurofibromas which subsequently progress to become MPNSTs. We hypothesized that comprehensively characterizing alterations in the genomes and gene expression profiles of peripheral nerve sheath tumors arising in our P_0-GGFβ3 mouse model will identify candidate driver genes mediating plexiform neurofibroma pathogenesis and neurofibroma-MPNST progression, thereby identifying new therapeutic targets in the equivalent human tumors. To test this overarching hypothesis, we are using a comprehensive multi-tiered process to identify candidate driver mutations in P_0-GGFβ3 neurofibromas and MPNSTs, establish gene signatures defining distinct tumor subtypes and functionally test the role of selected driver mutations characteristic of specific subtypes. Potential driver mutations within relatively large regions of chromosomal gain or loss will be identified using high density array comparative genomic hybridization (aCGH) and cross-species comparisons of this data with aCGH findings from human neurofibromas and MPNSTs. Smaller mutations (missense mutations, nonsense mutations, small indels and fusion events) will be identified using a combination of transcriptome (RNA-Seq) and exome sequencing in these same murine tumors. The contribution of selected candidate driver mutations characteristic of specific tumor subtypes will be validated by manipulating the function of these genes and examining the effect this has *in vivo*, using orthotopically allografted tumor cells, and a variety of *in vitro* functional assays. We will validate the relevance of these mutated mouse genes in human neurofibromas and MPNSTs by determining whether these same genes are mutated in human tumors.

BODY

This progress report covers progress made up to February, 2014, when Dr. Carroll left UAB to assume a position as Professor and Chair of the Department of Pathology and Laboratory Medicine at the Medical University of South Carolina (MUSC). This grant was not transferred to MUSC until September 15, 2015. The DOD has asked that a separate report be submitted (due June 30, 2016) that covers work made after the transfer to MUSC. Consequently, although we have made extensive additional progress since arriving at MUSC, that progress has not been incorporated into this report and will be instead be included in the June 2016 progress report. This report instead covers the approximately 6 months since the last progress report was filed.

Below, I will first indicate the two Specific Aims of our project and the tasks within each Aim. We have made extensive progress on the first task of Specific Aim 1, which has resulted in the generation of two high quality manuscripts, five abstracts and four presentations (see Reportable Outcomes); Stephanie Brosius, an M.D.-Ph.D. student in my laboratory, has also successfully defended her Ph.D. dissertation, which was based, in part, on this project. Please note that this progress is on track with our original approved Statement of Work as the majority of Task 2 of Specific Aim 1 and the experiments proposed in Specific Aim 2 are not scheduled to begin until the second year of the project; the sole exception was obtaining regulatory review and approval for these components, which has been successfully completed. Consequently, the work that I describe after I delineate the overall goals of this project will focus primarily (but not exclusively) on Task 1 of Specific Aim 1. In that description, I will first describe the work covered in the two manuscripts. I will then turn to our as yet unpublished data, linking each set of experiments to the different components of Task 1 of Specific Aims 1 and 2.

Specific Aim 1: Test the hypothesis that MPNST pathogenesis is driven by the accumulation of specific collections of multiple, as yet unknown, driver mutations.

Task 1. To perform aCGH, RNA-Seq and exome sequencing analyses of 40 early passage MPNST cultures derived from tumors developing in P_0-GGFβ3 mice (months 1-36):

a. Isolate RNA and genomic DNA from cultures suitable for analysis (months 1-12)
b. Perform aCGH experiments with genomic DNA isolated from the cultures (months 3-24)
c. Perform RNA-Seq experiments with RNA isolated from the cultures (months 3-24)
d. Perform exome sequencing experiments with genomic DNA isolated from the cultures (months 3-24)
e. Perform bioinformatic analyses of results from experiments described in a-d(months 3-36)

Task 2. Validate the role selected candidate driver genes play in tumorigenesis (months 8-36):

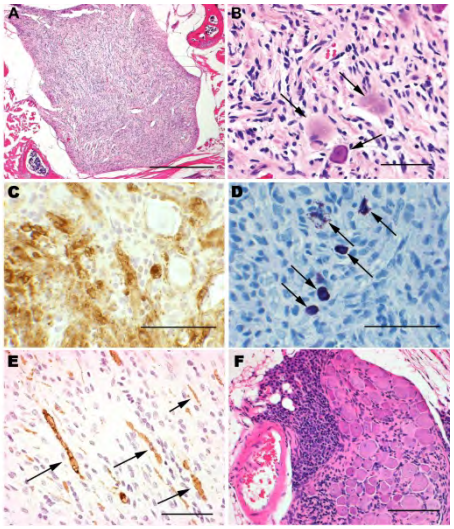

Figure 1. P_0-GGFβ3 mice develop multiple neurofibromas that may undergo malignant transformation. (A) Low power image of a neurofibroma developing on a dorsal spinal nerve root in a P_0-GGFβ3 mouse. Scale bar, 500 μm. (B) Higher power view of the tumor shown in A. *Arrows* indicate entrapped ganglionic neurons. (C) Tumor shown in A immunostained for S100β to demonstrate the coexistence of S100β-positive and -negative elements within this neoplasm. (D) An Unna's methylene blue stain performed on sections of the tumor shown in A demonstrates the presence of numerous mast cells evident by their prominent metachromasia (cells with dark purple granules, *arrows*). (E) Tumor immunostained with the anti-neurofilament antibody SMI34 to demonstrate axons (*arrows*) entrapped by infiltrating tumor cells. (F) Microscopic focus of apparent malignant transformation (markedly hypercellular region, left half of the field) arising in a spinal nerve root neurofibroma. Scale bar in B-F, 50 μm.

a. Obtain regulatory review and approval for these studies (months 8-12)

b. Extract expression level data from RNA-Seq experiments performed in task 1 to identify candidate genes (months 12-36)

c. Introduce lentiviruses expressing shRNAs targeting candidate genes into tumor cells and verify knockdown of target (months 12-36)

d. Orthotopically xenograft tumor cells transduced with candidate gene shRNA lentiviruses into immunodeficient mice and examine effect knockdown has on tumorigenesis (months 12-36)

e. Test effect candidate gene shRNA lentivirus transduction has on tumor cell proliferation, survival and migration (months 12-36)

Specific Aim 2: Test the hypothesis that plexiform neurofibroma pathogenesis is driven by the accumulation of specific collections of multiple, as yet unknown, driver mutations.

Task 3. To perform aCGH, RNA-Seq and exome sequencing analyses of 40 plexiform/intraneural neurofibroma-derived Schwann cultures established from tumors developing in P_0-GGFβ3 mice (months 12-36):

a. Isolate RNA and genomic DNA from cultures suitable for analysis (months 12-24)

b. Perform aCGH experiments with genomic DNA isolated from the cultures (months 12-36)

c. Perform RNA-Seq experiments with RNA isolated from the cultures (months 12-36)

d. Perform exome sequencing experiments with genomic DNA isolated from the cultures (months 12-36)

e. Perform bioinformatic analyses of results from experiments described in a-d (months 12-36)

Task 4. Validate the role selected candidate driver genes play in tumorigenesis (months 8-36):

f. Obtain regulatory review and approval for these studies (months 8-12)

g. Extract expression level data from RNA-Seq experiments performed in task 3 to identify candidate genes (months 12-36)

h. Introduce lentiviruses expressing shRNAs targeting candidate genes into tumor cells and verify knockdown of target (months 12-36)

i. Orthotopically xenograft tumor cells transduced with candidate gene shRNA lentiviruses into immunodeficient mice and examine effect knockdown has on tumorigenesis (months 12-36)

j. Test effect candidate gene shRNA lentivirus transduction has on tumor cell proliferation, survival and migration (months 12-36)

Our **first manuscript** (Kazmi SJ *et al* Transgenic mice overexpressing neuregulin-1 model neurofibroma-malignant peripheral nerve sheath tumor progression and implicate specific chromosomal copy number variations in tumorigenesis) was published in *The American Journal of Pathology*. In this manuscript, we rigorously characterized tumorigenesis in our P_0-GGFβ3 mouse model so as to convince the NF1 research community that this model appropriately modeled

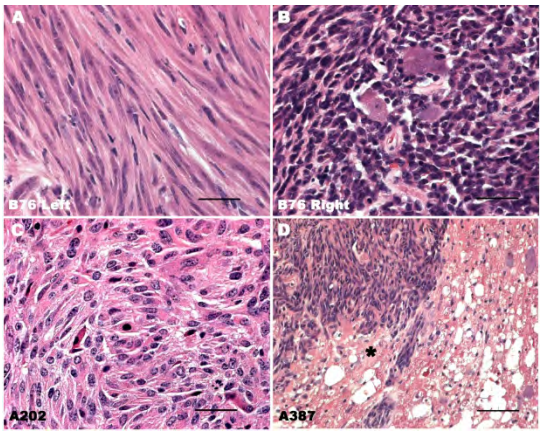

Figure 2. Representative images of MPNSTs arising in P_0-GGFβ3 mice, demonstrating the histologic variability encountered in these neoplasms. (A, B) Images illustrate the histology of tumors that arose independently in the left (A) and right (B) trigeminal nerves of mouse B76. Note the extreme spindled morphology of the tumor cells in A, which contrasts markedly with the densely packed, poorly differentiated cells composing the tumor seen in B. (C) MPNST with an epithelioid morphology that arose in the sciatic nerve of mouse A202. (D) A trigeminal MPNST from mouse A387 invading the undersurface of the brain. *, overlying brain parenchyma that is being invaded by this tumor. Scale bars in A-C, 50 μm; in D, 200 μm.

neurofibroma-MPNST progression and that the genomic abnormalities occurring in the MPNSTs arising in these mice paralleled those in their human counterparts and thus represented a valid model for our cross-species comparative oncogenomics studies. A summary of the key findings from this paper follows.

If MPNSTs arising in P_0-GGFβ3 mice develop via progression from pre-existing neurofibromas, neurofibromas should be evident in these animals. Since only a subset of these neurofibromas would be expected to accumulate the additional mutations required for progression, we would also predict that neurofibromas would be more common than MPNSTs in P_0-GGFβ3 mice. To test this, we established a cohort of 44 mice (21 females and 23 males) carrying the P_0-GGFβ3 transgene on an outbred C57BL/6J x SJL/J background and followed them until their death (mean age at death, 261.5 days; median, 220.5 days; range, 74-533 days). Complete necropsies were then performed. Peripheral nerve sheath tumors in these animals were evaluated using WHO diagnostic criteria for neurofibromas and MPNSTs (1). In most mice (41/44; 91%), virtually every dorsal spinal nerve root was markedly enlarged by intraneural tumor growth (Fig. 1A). These neoplasms were moderately cellular lesions that did not demonstrate the hypercellularity, increased nuclear size, hyperchromasia or increased mitotic activity seen in low grade MPNSTs. The tumors were predominantly composed of elongated cells with spindled nuclei (Fig. 1B) that diffusely infiltrated nerve roots and dorsal root ganglia, as demonstrated by the presence of entrapped neurons and axons (Fig. 1B, 1E). Immunoreactivity for the Schwann cell marker S100β was evident in a major population of intratumoral cells that were intimately intermingled with S100β-negative cells (Fig. 1C). These tumors also contained large numbers of mast cells (Fig. 1D). Similar neoplasms were present in the trigeminal ganglia and sympathetic nervous system of these P_0-GGFβ3 mice. Considered together, the histopathologic features of the low grade neoplasms occurring in the dorsal spinal nerve roots, trigeminal ganglia and sympathetic nervous system of P_0-GGFβ3 mice are identical to those seen in human neurofibromas.

We also found that 5 of the 44 mice had neurofibromas that contained small foci with a higher grade appearance (Fig. 1F). A comparison of these foci to the MPNSTs that developed in P_0-GGFβ3 mice (see below) showed a striking similarity between the atypical foci and many of the higher grade lesions found in these animals (e.g., compare the focus illustrated in Fig. 1F to the high grade tumors seen in Figs. 2B and 2D). This observation suggests that the neurofibromas developing in P_0-GGFβ3 mice are the precursors that ultimately give rise to MPNSTs in these animals.

MPNSTs were present in thirty-one (71%) of the necropsied P_0-GGFβ3 mice. These large tumors had a fleshy appearance, with areas of hemorrhage and necrosis often evident. Microscopic examination showed them to be markedly hypercellular with brisk mitotic activity and to be histologically similar to human MPNSTs (Fig. 2). Most of these MPNSTs were composed of closely packed, hyperchromatic cells with eosinophilic cytoplasm (Fig. 2B, D) and resembled the high grade tumors seen in our initial studies of these animals (2). With this larger sampling of tumors, however, it became apparent that the MPNSTs developing in P_0-GGFβ3 mice, like human MPNSTs (3), were morphologically diverse, with neoplasms that arose independently in the same animal sometimes differing markedly in appearance (e.g., compare the extreme spindled morphology of the tumor cells in the neoplasm which arose in the left trigeminal nerve of mouse B76 (Fig. 2A) to that of the densely packed, poorly differentiated cells evident in a tumor which arose in the right trigeminal nerve of this

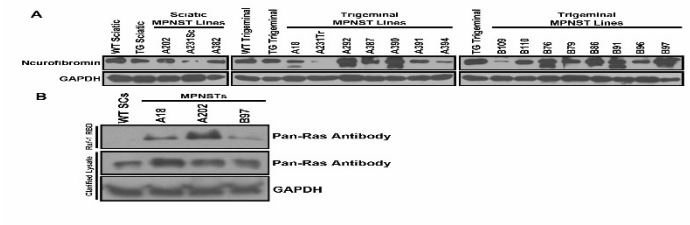

Figure 3. Although neurofibromin expression is typically maintained in P_0-GGFβ3 MPNSTs, Ras is hyperactivated in these neoplasms compared to wild-type Schwann cells. (A) Immunoblotted lysates of wild-type and transgenic non-neoplastic Schwann cells and 18 early passage P_0-GGFβ3 MPNST cultures probed for neurofibromin (1:500 antibody dilution). The 250 kDa form of neurofibromin is present in Schwann cells and the MPNST cells, with some MPNST cultures also demonstrating the 220 kDa splice variant of this protein. (B) The Raf-1 Ras-binding domain was used to pull down activated Ras protein in wild-type Schwann cells and three early passage P_0-GGFβ3 MPNST cultures. An immunoblot of the captured activated Ras proteins was then probed with a pan-Ras antibody that detects H-Ras, K-Ras and N-Ras (upper panel). The middle and lower panels are immunoblots of the clarified lysate prior to Ras pulldown probed with the pan-Ras antibody and an anti-GAPDH antibody, respectively.

same mouse (Fig. 2B)). Occasional MPNSTs even had an epitheloid appearance (Fig. 2C). Nonetheless, all of these tumors expressed S100β, as expected for MPNSTs. In contrast to the neurofibromas, which were confined to their nerve of origin, the MPNSTs were locally aggressive, commonly invading adjacent organs (Fig. 2D), soft tissue, bone, and skeletal muscle.

In comparison to neurofibromas, which typically occurred in large numbers in tumor-bearing P_0-GGFβ3 mice, MPNSTs were much less common. Twenty-three of the 31 mice (74%) with these higher grade neoplasms had only a single MPNST, with six animals (19%) having 2 MPNSTs and two (6%) having 3 or more (range: 3-5) high grade tumors. In 24 (77%) of the 31 P_0-GGFβ3 mice with MPNSTs, the neoplasms arose in trigeminal nerves. Spinal nerve roots and sciatic nerves were also common sites of MPNST occurrence [10/31 animals (32%)], with the remainder developing in the region of the superior cervical ganglion [2/31 mice (6.5%); these summed percentages exceed 100% because some animals developed multiple neoplasms]. MPNSTs occurred with similar frequencies in male [16/23 (70%)] and female [15/21 (71%)] mice.

We next examined P_0-GGFβ3 MPNSTs to determine whether they demonstrated *Nf1* and cell cycle regulatory abnormalities analogous to those commonly found in human MPNSTs. We focused on MPNSTs in these experiments for two reasons. First, MPNSTs represent the culmination of the neoplastic process in P_0-GGFβ3 mice and thus are the lesions most likely to demonstrate the full spectrum of driver mutations. Second, beyond a loss of *NF1*, mutations of tumor suppressors or other driver gene abnormalities have not yet been identified in human neurofibromas.

We first examined neurofibromin expression in cultures derived from these tumors. In these analyses, we compared expression in MPNST cells to that in transgenic non-neoplastic Schwann cells as this allowed us to identify changes in tumor suppressor and oncogene expression that were associated with tumor pathogenesis rather than transgene expression. Lysates of MPNST cultures and non-neoplastic Schwann cells derived from the nerve type (trigeminal or sciatic) in which the tumors arose were immunoblotted and probed with an antibody that recognizes both of the major neurofibromin splice variants (220 and 250 kDa). We found that neurofibromin expression in P_0-GGFβ3 MPNST cells was typically equal to or higher than that seen in non-neoplasic Schwann cells (Fig. 3A). Real-time PCR assays similarly showed little evidence of a reduction in *Nf1* mRNA levels.

We next asked whether P_0-GGFβ3 MPNST cells showed the Ras hyperactivation characteristic of human *NF1*$^{-/-}$ MPNST cells (4, 5). To compare the relative levels of activated Ras in non-neoplastic Schwann cells and three representative P_0-GGFβ3 MPNST cultures, a GST fusion protein containing the Raf1-Ras binding domain (RBD) was used to pull down activated Ras proteins from lysates of these cells. Proteins captured with the Raf1-RBD were immunoblotted and probed with a pan-Ras antibody that recognizes all three members (H-Ras, N-Ras, K-Ras) of the classic Ras subfamily. While activated Ras was undetectable in non-neoplastic Schwann cells, activated Ras was easily identified in P_0-GGFβ3 MPNST cells (Fig. 3B). Thus, although neurofibromin expression is maintained in P_0-GGFβ3 MPNSTs, these tumors, like neurofibromin-null human MPNSTs (5, 6), demonstrate Ras hyperactivation.

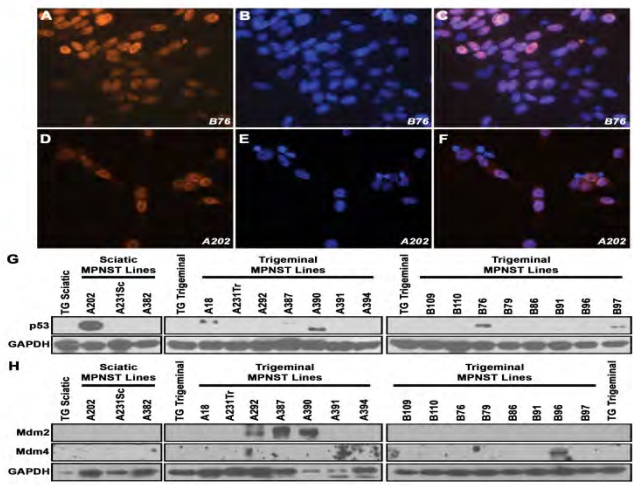

Figure 4. Abnormalities in the p19^{ARF}-Mdm-p53 signaling pathway occur in early passage P_0-GGFβ3 MPNST cultures. (A-F) Immunocytochemistry demonstrates intranuclear accumulation of p53 in two representative p53-overexpressing P_0-GGFβ3 MPNST early passage cultures. Panels A, D—p53 immunoreactivity (red-orange staining); panels B, E—bisbenzamide (nuclear) counterstain (blue); panels C, F—merged images of p53 immunoreactivity and bisbenzamide staining to demonstrate that p53 in these tumors cells accumulates within the nuclei. (G) Immunoblotted lysates of non-neoplastic transgenic Schwann cells and early passage cultures derived from 18 independently arising P_0-GGFβ3 MPNSTs probed for p53 (1:1000 dilution). Blots were reprobed with GAPDH to verify equivalent loading. (H) Immunoblotted lysates of non-neoplastic transgenic Schwann cells and early passage cultures derived from 18 independently arising P_0-GGFβ3 MPNSTs probed for Mdm2 (1;500 dilution, upper panels) or Mdm4 (1:500 dilution, middle panels). Blots were reprobed with GAPDH (lower panels) to verify equivalent loading.

To determine whether p53 abnormalities were present in P_0-GGFβ3 MPNSTs, we immunostained tumors and early passage cultures derived from these tumors for p53. Although p53 immunoreactivity was not uniformly present, it was evident in six of the eighteen neoplasms and early passage cultures derived from these neoplasms (Fig. 4A-F). This immunoreactivity was predominantly present in the nuclei of the tumor cells. To determine whether the presence of p53 immunoreactivity in these MPNSTs reflected tumor progression, we also immunostained a series of 13 P_0-GGFβ3 neurofibromas with an anti-p53 antibody. In contrast to the MPNSTs, none of the neurofibromas demonstrated p53 immunoreactivity.

To compare the levels of expression of p53 in P_0-GGFβ3 MPNSTs to that in non-neoplastic Schwann cells, lysates of Schwann cells from P_0-GGFβ3 mice and early passage MPNST cultures were immunoblotted and probed for p53. In both transgenic non-neoplastic Schwann cells (Fig. 4G) and wild type Schwann cells, p53 was undetectable. In contrast, MPNSTs with prominent nuclear p53 immunoreactivity (A202, A18, A387, A390, B76 and B97) all showed increased p53 expression in immunoblot analyses. The p53 immunoreactive species in these tumors had a mass of 53 kDa with the exception of tumor A390. In this latter neoplasm, the p53 antibody recognized a species with a lower molecular weight, suggesting the occurrence of a truncating mutation or a deletion.

To identify potential p53 mutations in these tumors, nested PCR was used to amplify *Trp53* sequences from eighteen early passage P_0-GGFβ3 MPNST cultures and the resulting products were sequenced in their entirety. In keeping with the size shift seen in immunoblots, the *Trp53* mRNA expressed in tumor A390 had a frameshift mutation in codon 314. We also found that tumor A202 expressed a transcript with a small in-frame deletion (codons 164-172) within the region encoding the p53 DNA binding domain. In tumor B76, a point mutation (c.R207C) was identified; Mutation Assessor (http://mutationassessor.org/), which assesses the likely impact of a mutation based on the nature of the change and whether it occurs in a conserved region, predicts that the c.R207C mutation has a high probability of impacting p53 function. Although tumor B97 showed no evidence of mutations within *Trp53* coding sequences, a 95 base pair duplication was evident in the 3' untranslated region of this mRNA. No *Trp53* mutations were identified in the p53-overexpressing A18 and A387 tumors or in any of the tumors lacking p53 overexpression. Thus, 33% (6/18) of the P_0-GGFβ3 MPNSTs we examined have abnormal expression or mutation of p53.

Dysregulation of the p19^{ARF}-Mdm-p53 pathway can also be caused by overexpression of Mdm2 or Mdm4. To determine whether Mdm2 or Mdm4 overexpression occurs in P_0-GGFβ3 MPNSTs, lysates of non-neoplastic Schwann cells from the sciatic and trigeminal nerves of P_0-GGFβ3 mice and early

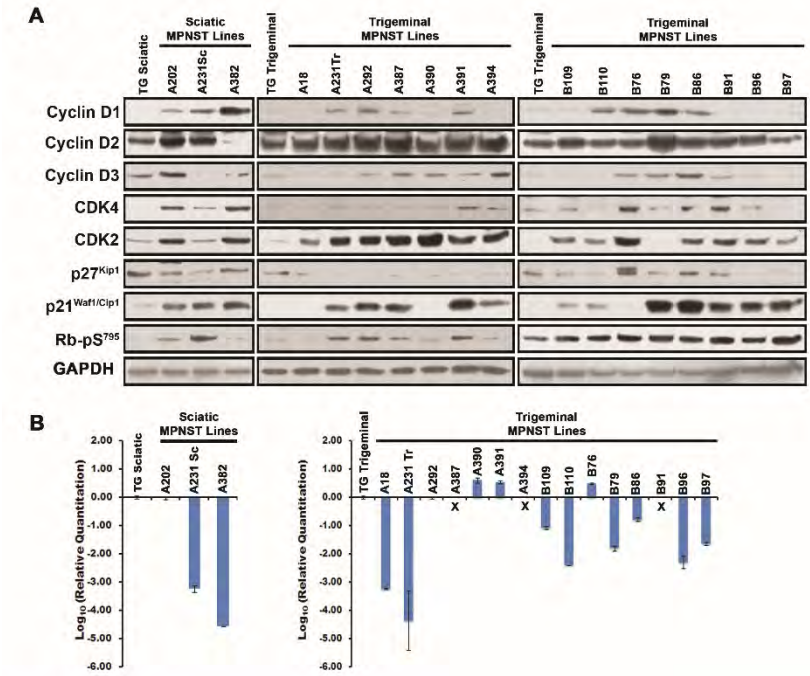

Figure 5. Abnormalities in cell cycle regulatory proteins are common in early passage cultures of P_0-GGFβ3 MPNST cells, but these cells are persistently dependent on aberrant growth factor signaling. (A) Immunoblotted lysates of non-neoplastic transgenic Schwann cells and early passage cultures of P_0-GGFβ3 MPNST cells probed for cyclin D1 (1:300 dilution), cyclin D2 (1:500 dilution), cyclin D3 (1:700 dilution), CDK4 (1:500 dilution), CDK2 (1:400 dilution), $p27^{Kip1}$ (1:600 dilution), $p21^{Cip1}$ (1:500 dilution), or Rb phosphorylated on Ser^{795} (1:700 dilution). The detected antigen is indicated to the left of each row of panels, while the identity of the cultures is indicated above each sample. Blots were reprobed with GAPDH to verify equivalent loading. (B) Real-time PCR analyses of *Cdkn2a* expression in non-neoplastic transgenic Schwann cells and early passage cultures of P_0-GGFβ3 MPNST cells. Transcript levels were normalized to levels detected in non-neoplastic transgenic Schwann cells. An "X" below a culture indicates that *Cdkn2a* transcripts were undetectable in the culture. Note that normalized *Cdkn2a* transcript levels are on a $\log_{10}$ scale.

passage tumor cultures were lysed, immunoblotted and probed for these two molecules. Mdm2 and Mdm4 were undetectable in non-neoplastic transgenic Schwann cells (Fig. 4H). In contrast, three of the MPNST early passage cultures (A292, A387 and A390) demonstrated prominent Mdm2 overexpression; the positive specimens include two tumors (A387, A390) that also had p53 overexpression. Mdm4 overexpression was evident in one tumor (B96). These results suggest that the $p19^{ARF}$-Mdm-p53 pathway is dysregulated by Mdm2 or Mdm4 overexpression in some P_0-GGFβ3 MPNSTs.

In human MPNSTs, the $p16^{INK4A}$-cyclin D/CDK4-Rb signaling pathway is often dysregulated (7-15). This can occur via multiple mechanisms including CDK4 overexpression, a loss of Rb expression or inappropriate Rb phosphorylation secondary to $p16^{INK4A}$ mutation, CDK4 overexpression or overexpression of D-cyclins. Lysates of non-neoplastic P_0-GGFβ3 Schwann cell and early passage P_0-GGFβ3 MPNST cultures were immunoblotted and probed for proteins within this pathway. Cyclins D1, D2 and D3 were all detectable in at least some MPNSTs (Fig. 5A) and were often expressed at levels higher than those evident in non-neoplastic Schwann cells. Overexpression of CDK4 was also seen in some tumors (e.g., A202, A382, B76 and B91). As our preliminary experiments indicated that detection of $p16^{INK4A}$ protein was problematic even in non-neoplastic Schwann cells, we instead used real-time PCR to quantify levels of the *Cdkn2a* mRNA encoding this protein in our cultures (Fig. 5B). Relative to non-neoplastic transgenic Schwann cells, *Cdkn2a* mRNA expression was decreased tenfold to more than ten thousand fold in ten tumors and was completely undetectable in three other tumors (A387, A394 and B91). Rb protein and mRNA levels were unchanged in these P_0-GGFβ3 MPNSTs (not shown). However, in keeping with the fact that D-cyclin overexpression, CDK4 overexpression and/or $p16^{INK4A}$ loss was present in most of the tumors, levels of Rb phosphorylated on Ser^{795} (a modification which promotes cell cycle progression) were increased in the majority of these MPNSTs (Fig. 5A). Thus, dysregulation of the $p16^{INK4A}$-cyclin D/CDK4-Rb pathway is quite common in P_0-GGFβ3 MPNSTs, much like their human counterparts.

Expression of $p21^{Cip1/Waf1}$ and $p27^{Kip1}$ is also lost in some human MPNSTs (13, 16, 17). We therefore examined our early passage P_0-GGFβ3 MPNST cultures to determine whether they had similarly lost these cell cycle inhibitors. Expression of $p27^{Kip1}$, but not $p21^{Cip1/Waf1}$, was commonly decreased in comparison to non-neoplastic Schwann cells (Fig. 5A). Interestingly, CDK2, a key target

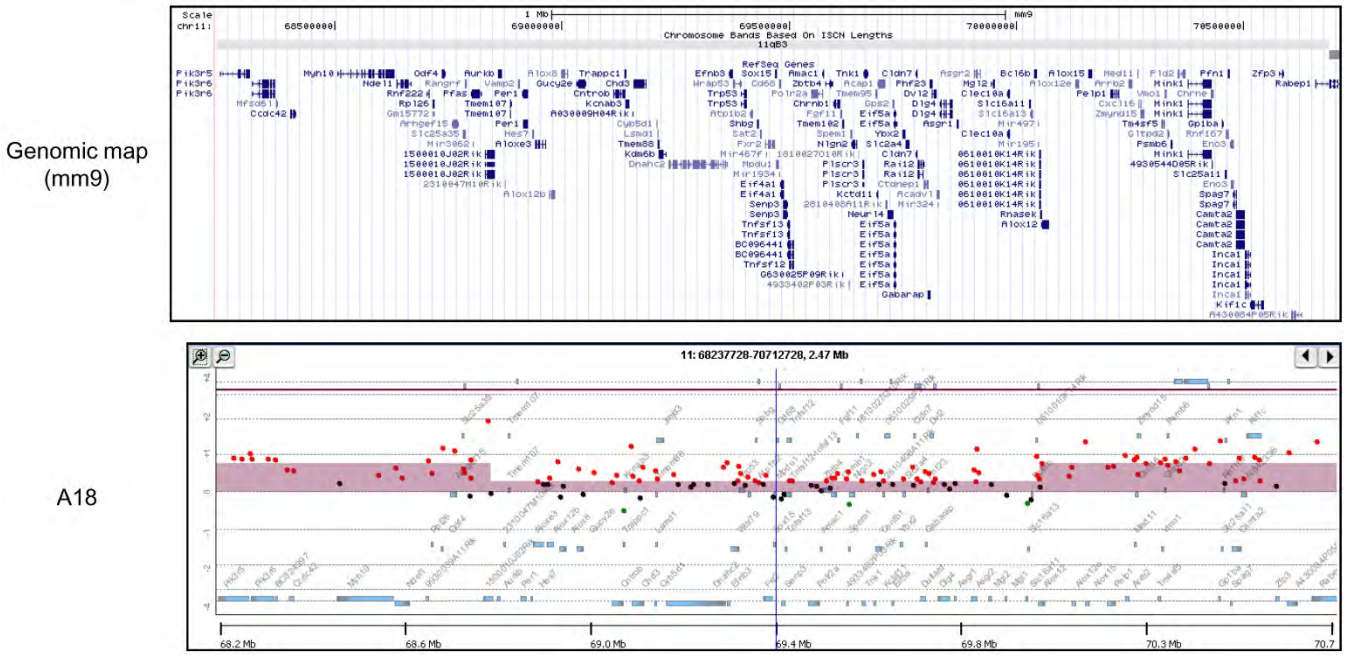

Figure 6. Array CGH analysis of the 2.47 Mb region in chromosome 11 encoding the Trp53 tumor suppressor gene in P_0-GGFβ3 MPNST A18. The lower panel indicates the relative signals in tumor (red) and non-neoplastic Schwann cell (green) DNAs, with the height of the colored bar indicating the relative difference in these two signals. Note the central 1.21 Mb region in which there is a relative copy number loss in the tumor. The upper panel indicates the location of the genes present within the region illustrated in the lower panel.

of $p27^{Kip1}$ and $p21^{Cip1/Waf1}$, was also overexpressed in sixteen of the eighteen tumors (Fig. 5A). These findings provide further evidence that cell cycle progression is dysregulated in P_0-GGFβ3 MPNSTs.

We hypothesized that an examination of other genomic abnormalities in P_0-GGFβ3 MPNSTs could potentially identify additional, previously unknown driver genes involved in the pathogenesis of these sarcomas. To test this possibility, genomic DNAs isolated from eleven P_0-GGFβ3 MPNST early passage cultures and cultured non-neoplastic non-transgenic Schwann cells were was labeled and hybridized to high density aCGH microarrays. The relative ratios of the signals from each genomic DNA were then compared to identify regions of unbalanced chromosomal gain or loss.

Copy number variations (CNVs) affecting whole chromosomes or entire chromosome arms were common in P_0-GGFβ3 MPNSTs, occurring on average 5.3 times (median, 4; range, 3-10) in each tumor genome (Table 1). Unbalanced gains predominated (average, 4 per genome; median, 3; range: 2-7), with whole chromosome gains evident in every MPNST examined. However, the distribution of these unbalanced gains was nonrandom. All eleven of the early passage MPNST cultures demonstrated gains of chromosome 11. Gains of chromosome 17 and the X chromosome were also common, occurring in five of the eleven cultures. Gain of chromosomes 1, 3, 6, 7, 12, 15, 16 and 19 was observed in multiple tumors, albeit at a lower rate. In contrast, unbalanced losses (average, 2.8 per genome in affected tumors; median, 1; range, 1-7) of whole chromosomes or chromosome arms were less common, occurring in only five P_0-GGFβ3 MPNSTs. These losses were also nonrandom, with unbalanced losses of chromosomes 9, 14, 16 and 19 identified in multiple tumors.

The observation that chromosome 11 was uniformly amplified in the P_0-GGFβ3 MPNSTs we examined was curious, as this murine chromosome carries the *Nf1* and *Trp53* genes, whose equivalents are commonly lost in human MPNSTs. We therefore examined chromosome 11 in more detail to determine whether smaller areas of unbalanced loss affecting either the *Nf1* or *Trp53* genes were present. Consistent with our observation that neurofibromin expression is maintained in these tumors, we found no evidence of small losses affecting the *Nf1* locus in any of the 11 tumors studied with aCGH. However, one tumor (A18) showed a relative loss of a 1.21 Mb segment (chr11:68,846,711-70,058,031) containing the *Trp53* gene (Fig. 6). This finding, combined with our mutational analyses of *Trp53* suggests that the $p19^{ARF}$-Mdm-p53 cascade in tumor A18 was impaired by both mutation of a *Trp53* allele and an overall reduction in *Trp53* copy number. Unbalanced losses affecting the *Trp53* gene were not evident in any of the other 10 MPNSTs we studied.

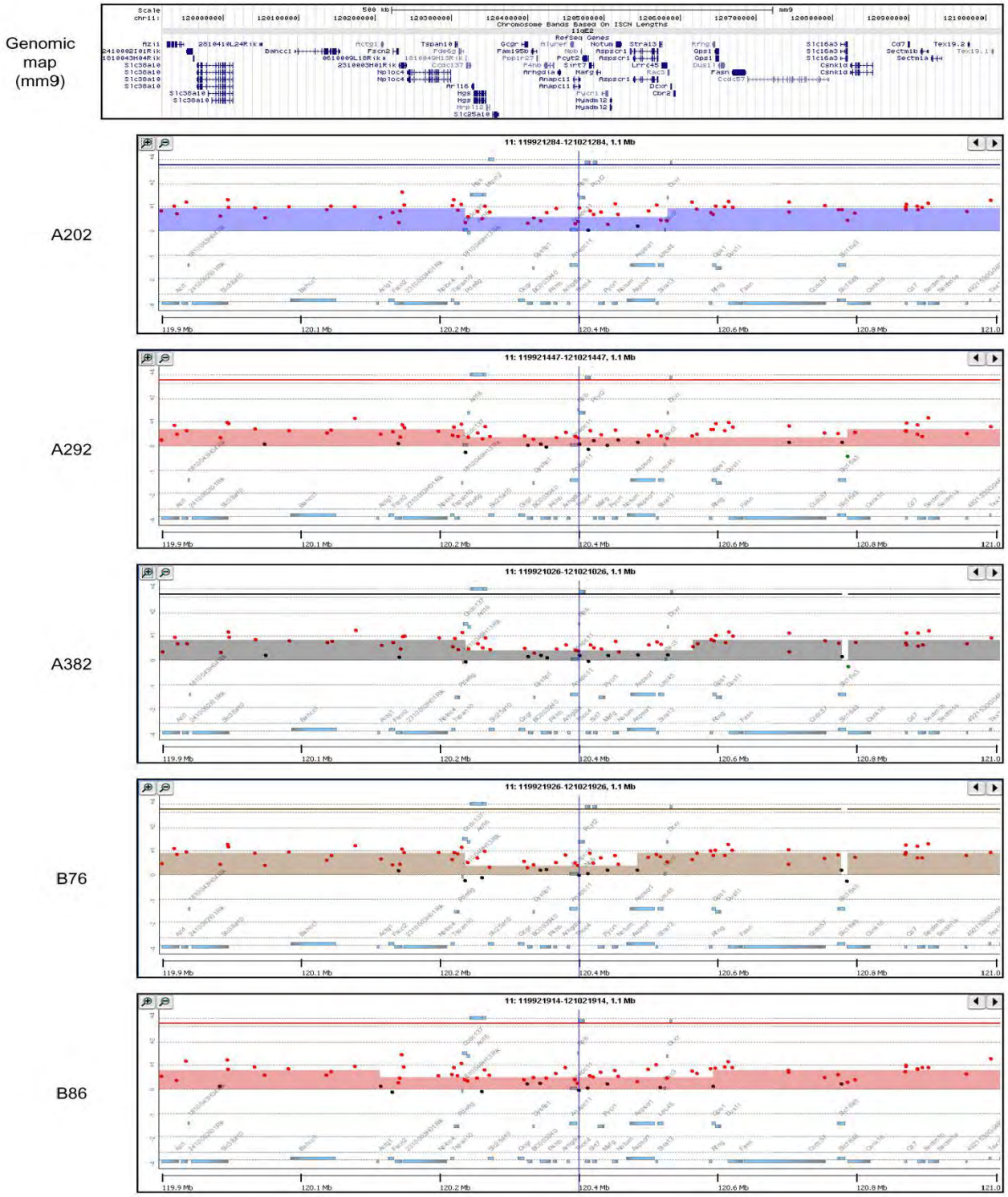

Figure 7. Array CGH analyses of a 1.1 Mb region in chromosome 11 that surrounds a region of relative copy number loss present in five P_0-GGFβ3 MPNSTs. The lower panels indicate the relative signals in tumor (red) and non-neoplastic Schwann cell (green) DNAs, with the height of the colored bar indicating the relative difference in these two signals; the identity of the tumors is indicated to the left of each panel. Note the variably sized central regions in which there is a relative copy number loss in these five tumors. The uppermost panel indicates the location of the genes present within the region illustrated in the lower panels.

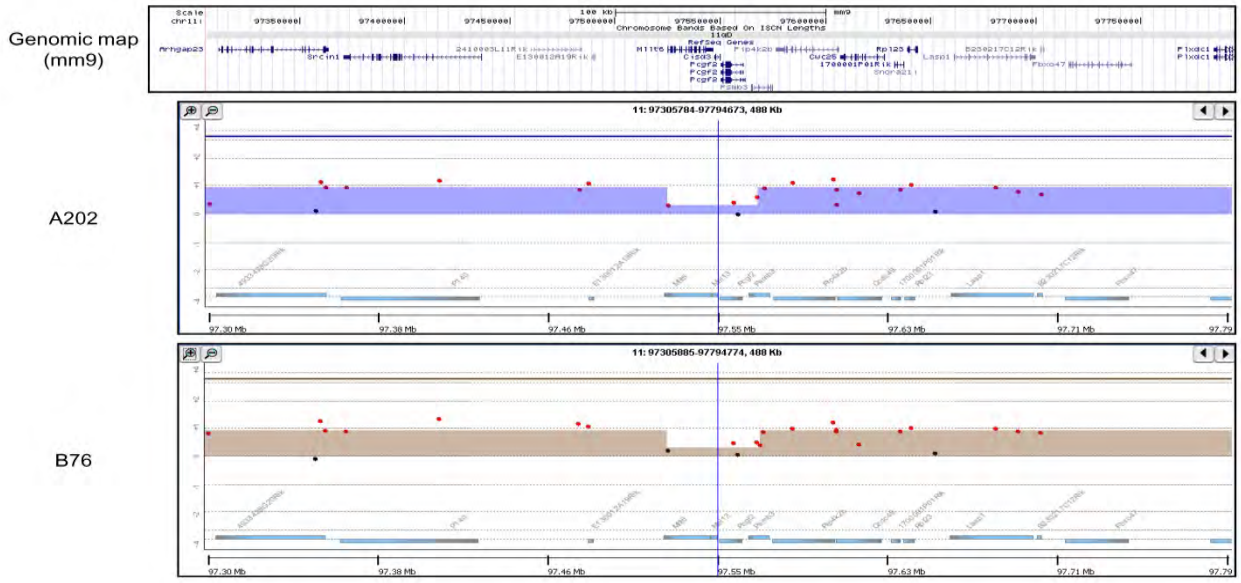

Figure 8. Array CGH analysis of a 488 kb region in chromosome 11 that surrounds a region of relative copy number loss present in P_0-GGFβ3 MPNSTs A202 and B76. The lower panels indicate the relative signals in tumor (red) and non-neoplastic Schwann cell (green) DNAs, with the height of the colored bar indicating the relative difference in these two signals; the identity of the tumors is indicated to the left of each panel. Note the central 44 kb region in which there is a relative copy number loss in these two MPNSTs. The upper panel indicates the location of the genes present within the region illustrated in the lower panels.

While examining chromosome 11, we also noted two other small areas of relative loss that were present in multiple P_0-GGFβ3 MPNSTs. Five tumors (A202, A292, A382, B76 and B86) showed a relative copy number loss which overlapped in a 225 kb region on chromosome 11 (chr11: 120,322,621-120,548,454; Fig. 7) that includes 24 known genes. To identify candidate driver genes in this interval, we compared these genes to the online comprehensive lists of driver genes available from the Atlas of Genetics and Cytogenetics in Oncology and Haematology (18), CANgenes (19), CIS(20) and the Sanger Cancer Gene Census (21). We found that two genes within this interval [*Mafg* (v-maf oncogene homolog G) and *Aspscr1* (alveolar soft part sarcoma chromosome region, candidate 1)] have been previously identified as genes that were affected in other cancer types. In addition, a 44 kb region (chr11: 97,526,341-97,570,620) containing four genes (*Mllt6*, *Cisd3*, *Pcgf2* and *Psmb3*) also showed a relative reduction in copy number in tumors A202 and B76 (Fig. 8). Examination of the databases noted above showed that one gene within this interval, *Mllt6*, has been previously implicated in the pathogenesis of acute myelocytic leukemias (22). Considered together, these observations suggest that multiple regions of relative copy number loss on chromosome 11 affect genes potentially relevant to MPNST pathogenesis.

Unlike human cancers, mouse cancer genomes tend to have whole chromosome gains or losses with only a limited number of small CNVs. However, those small regions of unbalanced gain or loss that do occur in murine cancers develop under strong selective pressure, implying that they contain important driver genes (23). Thus, we next focused our attention on the small CNVs occurring in P_0-GGFβ3 MPNSTs. In our eleven early passage MPNST cultures, 44 focal regions of unbalanced chromosomal gain and loss were evident. These small CNVs, which included 26 unbalanced gains and 18 unbalanced losses, were spread across 15 chromosomes (Fig. 9). Several of the small CNVs were evident in multiple P_0-GGFβ3 MPNSTs (Table 2). For instance, a deletion on chromosome 4 was present in six of the eleven tumors; this region of chromosomal loss (chr4: 88,934,158-89,039,587) contains the *Cdkn2a*/*Cdkn2b* gene. A global examination of the focal CNVs present in these P_0-GGFβ3 MPNSTs showed that genes represented in the Atlas of Genetics and Cytogenetics in

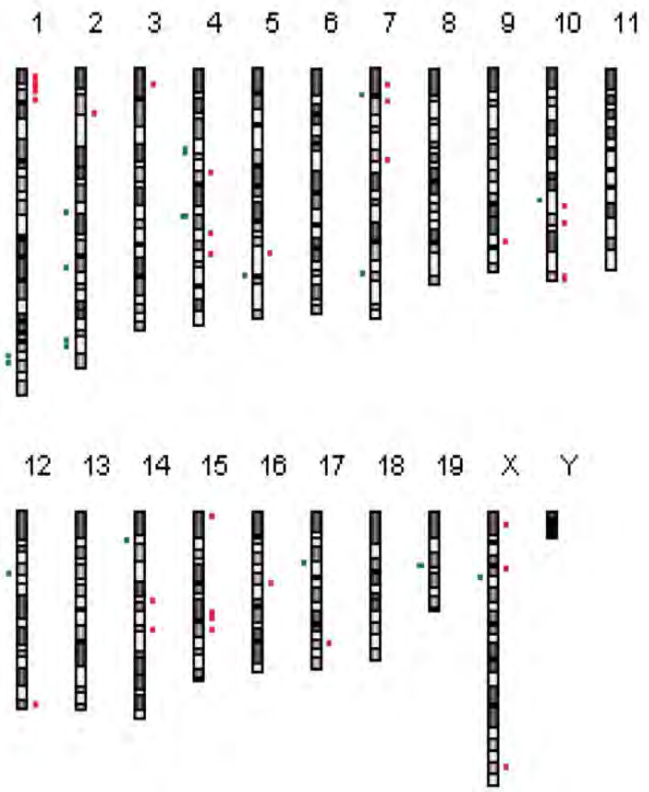

Figure 9. Ideogram indicating the locations of focal CNVs detected by array CGH data in early passage cultures established from P_0-GGFβ3 MPNSTs. Regions of copy number gain are indicated in red, while regions of unbalanced loss are indicated in green. The lengths of the red and green bars are proportional to the size of the CNV.

Oncology and Haematology, CANgenes, CIS or Sanger Cancer Gene Census databases were evident in 22 of the 44 regions (13 amplified, 9 deleted; these genes are bolded and underlined in Table 2). Overall, 39 genes previously implicated in the pathogenesis of other human cancer types were identified within these regions (1-8 genes per focal CNV).

The functions of the candidate cancer driver genes present within focal CNVs in P_0-GGFβ3 MPNSTs were variable and impacted multiple processes relevant to tumorigenesis (Table 3). A number of the affected loci encoded proteins that control proliferation (*Myc, Tpd52, Strn*; all amplified), the cell cycle (*Cdkn2a*, *Cdkn2b*, *Chfr*, *Chek2*, *Cdk2ap1*, *Cdk4*) and chromatin remodeling (*Ep400*). Several genes regulating apoptosis (*Bbc3/PUMA*, *Ddit3/GADD153*, *XIAP*) were also present within focal areas of unbalanced gain or loss. Genes encoding molecules in key cytoplasmic signaling pathways including the Hippo (*Stk4*), Notch (*Dtx3*), Hedgehog (*Gli1*), Arf (*Agap2*), Rho (*Arhgap9*), PI3 kinase (*Pten*) and Myc (*Myc*) pathways as well as genes for growth factors, cytokines and growth factor receptors potentially upstream of some of these signaling cascades (the growth hormone receptor gene *Ghr*, *Il17a*, *Inhbe*) were additionally affected. Other candidate cancer driver genes within these small CNVs function in key metabolic pathways (*Aldob*, *Mars*, *Alad*), transcriptional control (*Ncoa3*, *Nr4a3*, *Zscan22*), vesicular trafficking (*Napa*) and cell motility (*Sept6*, *Vcl*).

It was also notable that some small CNVs that did not contain genes previously implicated in the pathogenesis of any tumor type were repeatedly identified in P_0-GGFβ3 MPNSTs (Table 2). The most common of these was a region of copy number gain on chromosome 4 (chr4: 111,745,189-112,130,291) that was present in ten out of the eleven tumors examined. This region contains three genes (*Skint4*, *Skint3* and *Skint9*) whose function is poorly understood; *Skint1*, the prototypic member of this group of molecules has been implicated in the maturation of epidermal γδ T-cells (24). Other recurrent CNVs lacking genes previously implicated in the pathogenesis of human cancers included a region of deletion on chromosome 17 that occurred in five of eleven tumors (chr17: 30,714,112-31,047,626, which includes the *Glo1*, *Dnahc8*, AKO18977 and *Glp1R* loci), a focal gain on chromosome 14 that was present in five of eleven tumors (chr14: 69,877,095-69,987,156; encompasses the *Slc25a37* and *Entpd4* genes) and a small deletion on chromosome 1 that was evident in five tumors (chr1: 173,444,742-173,494,144; includes the *Itln1* and *Cd244* genes). Considered together, these observations suggest that several of the relatively small regions of chromosomal copy number gain or loss evident in P_0-GGFβ3 MPNSTs contain important driver genes that have not been previously implicated in carcinogenesis.

Although our initial manuscript clearly indicated that the MPNSTs arising in P_0-GGFβ3 mice recapitulated most of the genomic abnormalities characteristic of human MPNSTs, it was notable that these tumors typically did not have *Nf1* mutations. This raised the question of whether these mutations were absent because NRG1 operated within the same pathway as *Nf1* (a question that is highly relevant to the significance of this model) or instead promoted neoplasia primarily via its effects on

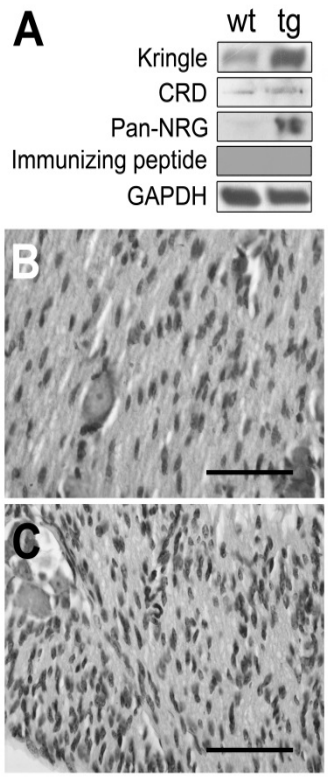

Fig. 10. Transgene expression and Schwann cell hyperplasia is maintained in P_0-GGFβ3 mice bred for >15 generations onto a C57BL/6J background. **A:** Immunoblot analyses of the levels of type II NRG1 protein detected with an anti-kringle domain antibody (*Kringle*), type III NRG1 protein detected with an anti-CRD domain antibody (*CRD*) and global NRG1 expression as detected with an antibody recognizing the EGF-like domain present in all biologically active NRG1 isoforms (*pan NRG*). Incubation of with an immunizing peptide ablates the signal from the anti-kringle domain antibody (*Immunizing peptide*). To verify equal protein loading, the blots were reprobed with an anti-GAPDH antibody (*GAPDH*). **B:** Hematoxylin and eosin stained preparations of trigeminal nerve from 1 month old wild-type and **C:** P_0-GGFβ3 mice. Note the increased cellularity (hyperplasia) in the P_0-GGFβ3 nerve relative to the wild-type nerve. Scale bars, 50μm.

other non-*Nf1* associated signaling pathways. Our **second manuscript** (Brosius SN *et a*l Neuregulin-1 overexpression and *Trp53* haploinsufficiency cooperatively promote *de novo* malignant peripheral nerve sheath tumor pathogenesis) was directed towards answering this question. This manuscript has been favorably reviewed by *Acta Neuropathologica*. We are currently addressing the criticisms raised by the three reviewers and will be resubmitting the revised version of this manuscript within the next 8 weeks. The following summarizes key findings from this manuscript.

This manuscript had its genesis in our fortuitous observation that mice carrying the P_0-GGFβ3 transgene on a C57BL/6J background maintained transgene expression and Schwann cell hyperplasia but fail to develop neurofibromas or MPNSTs. We have previously reported that P_0-GGFβ3 mice have a shortened lifespan (average survival, 262 days), develop both neurofibromas and MPNSTs at a high frequency on an outbred C57BL/6J x SJL/J background or when bred onto a C57BL/6J background for 5-8 generations and recapitulate the process of neurofibroma-MPNST progression seen in human NF1 patients (2, 25). However, when we bred P_0-GGFβ3 mice on a C57BL/6J background for 15 or more generations (referred to below as an inbred C57BL/6J background), we found that they survived without obvious abnormalities to 1 year of age and no longer developed tumors. To determine why tumorigenesis was lost in mice carrying the P_0-GGFβ3 transgene on an inbred C57BL/6J background, we compared NRG1 expression in the trigeminal nerves of wild-type C57BL/6J mice to that in P_0-GGFβ3 mice at 1 month of age, a time which represents the peak of Schwann cell hyperplasia in P_0-GGFβ3 mice (2). Lysates of these nerves were immunoblotted and probed with antibodies recognizing either the kringle domain located at the N-terminus of type II (GGF) NRG1 isoforms, the CRD domain found only in type III NRG1 isoforms or the EGF-like common domain present in all NRG1 proteins (a pan-NRG1 antibody). The anti-CRD domain antibody showed similar levels of type III NRG1 protein in wild-type and P_0-GGFβ3 trigeminal nerve (Fig. 10A). In contrast, both the anti-kringle domain and the pan-NRG1 antibodies demonstrated higher levels of expression of a 54 kDa species (the expected size of GGFβ3) in transgenic animals compared to wild-type controls. Thus, a suppression of transgene expression was not responsible for the loss of tumorigenesis in these mice.

To determine whether Schwann cell hyperplasia still occurred in P_0-GGFβ3 mice on an inbred C57BL/6J background, we compared the histology of sciatic and trigeminal nerves collected from 1 month old wild-type C57BL/6J mice to that of the same nerves from P_0-GGFβ3 mice. We found that Schwann cell hyperplasia was indeed still present in nerves from P_0-GGFβ3 mice (Fig. 10B, C). Thus, mice carrying the P_0-GGFβ3 transgene on an inbred C57BL/6J background still develop Schwann cell hyperplasia. However, on an inbred C57BL/6J genetic background, these preneoplastic peripheral nervous system abnormalities do not advance to tumorigenesis.

Our observation that tumorigenesis is suppressed in P_0-GGFβ3 mice on an inbred C57BL/6J background gave us the

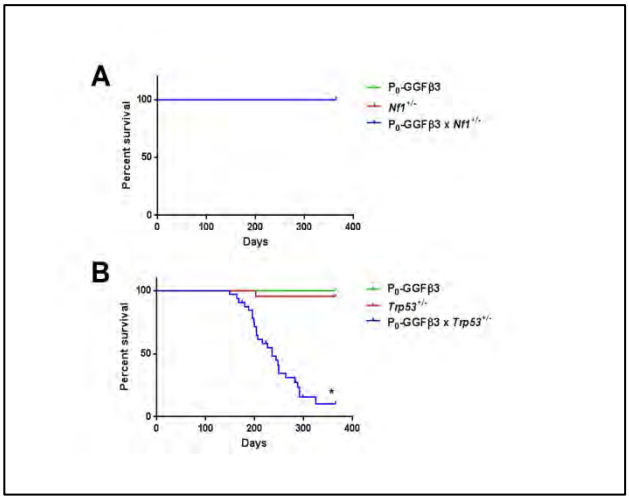

Fig. 11. Haploinsufficiency for *Trp53*, but not *Nf1*, impairs survival in the presence of NRG1 overexpression. **A:** Kaplan-Meier curve indicating the survival rates of P_0-GGFβ3, *Nf1*$^{+/-}$ and P_0-GGFβ3;*Nf1*$^{+/-}$ mice over the first year of life. No decrease in survival is seen for any of these cohorts. **B:** Kaplan-Meier curve indicating the survival rates of P_0-GGFβ3, *Trp53*$^{+/-}$ and P_0-GGFβ3;*Trp53*$^{+/-}$ mice over the first year of life. While the survival of P_0-GGFβ3 and *Trp53*$^{+/-}$ mice is unimpaired over this interval, the survival of P_0-GGFβ3;*Trp53*$^{+/-}$ mice is significantly shortened (average survival, 226 days). *, *p*-value<0.0001.

opportunity to assess the relationship between NRG1 and *Nf1* loss via genetic complementation. We reasoned that if NRG1 promotes tumorigenesis primarily by activating essential signaling cascades that parallel those affected by *Nf1* loss, then crossing P_0-GGFβ3 mice to *Nf1*$^{+/-}$ mice could potentially "unmask" tumorigenesis, resulting in the reappearance of neurofibromas and/or MPNSTs in these animals. If, on the other hand, the primary tumorigenic effect of NRG1 overexpression in Schwann cells was modulation of *Nf1*-regulated signaling cascades, then NRG1 overexpression should substitute for *Nf1* loss. In this circumstance, the phenotype of P_0-GGFβ3;*Trp53*$^{+/-}$ mice would be analogous to that of *cis-Nf1*$^{+/-}$;*Trp53*$^{+/-}$ mice which develop MPNSTs *de novo* rather than from a pre-existing neurofibroma (26, 27). To evaluate these alternatives, we bred mice carrying the P_0-GGFβ3 transgene on an inbred C57BL/6J background to animals with the same genetic background that were haploinsufficient for either *Trp53* (*Trp53*$^{+/-}$ mice) or *Nf1* (*Nf1*$^{+/-}$ mice). Cohorts of P_0-GGFβ3, *Nf1*$^{+/-}$, *Trp53*$^{+/-}$, P_0-GGFβ3;*Nf1*$^{+/-}$ and P_0-GGFβ3;*Trp53*$^{+/-}$ mice (20 mice of each genotype, with each cohort containing an equal number of males and females) were then followed until death or one year of age. We found that P_0-GGFβ3, *Nf1*$^{+/-}$, and P_0-GGFβ3; *Nf1*$^{+/-}$ mice showed no reduction in survival over the first year of life (Fig. 11A). The survival of the *Trp53*$^{+/-}$ cohort was only slightly and non-significantly lowered due to the death of a single animal (average survival, 357 versus 365 days; Fig. 11B). However, there was a significant decrease when comparing the Kaplan-Meier survival curves of P_0-GGFβ3;*Trp53*$^{+/-}$ mice (average survival, 226 days) to those of P_0-GGFβ3 and *Trp53*$^{+/-}$ mice (Fig. 11B; *, *p*<0.0001 based on a log-rank test); only one P_0-GGFβ3;*Trp53*$^{+/-}$ mouse survived to 1 year of age. There was no difference in the survival of male and female mice within the P_0-GGFβ3;*Trp53*$^{+/-}$ cohort.

We then performed complete necropsies on each of the cohorts described above. There was no evidence of neurofibromas, MPNSTs or any other tumor type in any of the P_0-GGFβ3, *Nf1*$^{+/-}$, or P_0-GGFβ3;*Nf1*$^{+/-}$ mice. Likewise, there was no evidence of neoplasia in any of the *Trp53*$^{+/-}$ mice except for the single animal that died early; we found a large fibrosarcoma in that mouse. In contrast, 95% (18/19) of the mice in the P_0-GGFβ3;*Trp53*$^{+/-}$ cohort had peripheral nervous system neoplasms (Table 4). The majority of these tumors were associated with trigeminal nerves (11/19; 58%) or dorsal spinal nerve roots (13/19; 68%), with a smaller number of neoplasms identified in the sciatic nerve (2/19; 11%). Within the P_0-GGFβ3;*Trp53*$^{+/-}$cohort, many of the tumor bearing animals presented with a single tumor. However, 53% (10/19) of the mice had multiple tumors, with a maximum of 5 neoplasms observed in an individual animal.

To establish whether these lesions arising in arising in P_0-GGFβ3;*Trp53*$^{+/-}$ mice were peripheral nerve sheath tumors or some other tumor type, we performed an extensive characterization of their tumors. We found that the tumors arising in P_0-GGFβ3;*Trp53*$^{+/-}$ mice had a similar histologic appearance. These markedly hypercellular neoplasms lacked the mixture of multiple cell types characteristic of neurofibromas, instead being uniformly composed of closely packed, atypical spindled cells which contained enlarged elongated nuclei with coarse chromatin (Fig. 12A). Brisk mitotic activity was evident in the tumors (Fig. 12A, arrows) and tumor necrosis was commonly seen (Fig. 12B, asterisk). These neoplasms were also highly aggressive, often invading adjacent bone (Fig. 12D) and soft tissues. The tumors found in P_0-GGFβ3;*Trp53*$^{+/-}$ mice were immunoreactive for S100β (Fig. 12D), consistent with an origin from the Schwann cell lineage. As immunoreactivity for both S100β and nestin

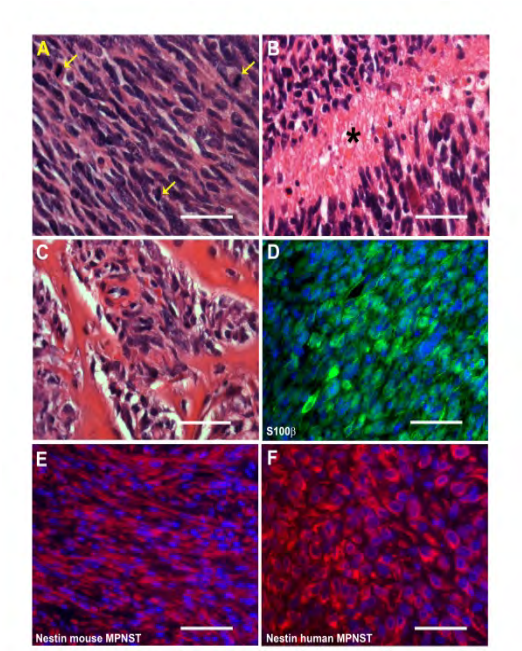

Fig. 12 P_0-GGFβ3;*Trp53*$^{+/-}$ mice develop MPNSTs, but not neurofibromas. **A-C:** Hematoxylin and eosin stained sections of MPNSTs arising in P_0-GGFβ3;*Trp53*$^{+/-}$ mice demonstrating the brisk mitotic activity (A, arrows) and tumor necrosis (B, asterisk) typically seen in these tumors. These tumors were highly aggressive, as demonstrated by their tendency to invade bone (C) and other adjacent structures. **D:** S100β immunoreactivity in an MPNST found in a P_0-GGFβ3;*Trp53*$^{+/-}$ mouse. **E-F:** Nestin immunoreactivity in a P_0-GGFβ3;*Trp53*$^{+/-}$ MPNST (E) compared to that seen in a human MPNST (F). Scale bars, 50μm.

distinguishes MPNSTs from other histologically similar sarcomas (28, 29), we also examined nestin expression in P_0-GGFβ3;*Trp53*$^{+/-}$ tumors. We found that the mouse tumors (Fig. 12E), like human MPNSTs (Fig. 12F), were strongly nestin positive.

Neurofibromas were extraordinarily rare in P_0-GGFβ3;*Trp53*$^{+/-}$ mice; we found only a single neurofibroma in one mouse within this cohort. This is quite different from outbred P_0-GGFβ3 mice, which had multiple neurofibromas in almost all of the mice we examined (25). This suggested that the MPNSTs arising in P_0-GGFβ3;*Trp53*$^{+/-}$ mice arose *de novo* rather than from pre-existing plexiform neurofibromas. As the trigeminal nerves and dorsal spinal nerve roots were the most common sites where we found MPNSTs in P_0-GGFβ3;*Trp53*$^{+/-}$ mice, we carefully examined these nerves and their associated ganglia to determine whether small nascent tumors were present within these structures. We found that 47% (9/19) P_0-GGFβ3;*Trp53*$^{+/-}$ mice had one or more microtumors in their trigeminal nerves or dorsal spinal nerve roots. Strikingly, these microtumors were uniformly located within the trigeminal or dorsal root ganglia (Fig. 13A). The microtumors had a histologic appearance similar to that of the larger MPNSTs described above, being evident as moderately hypercellular proliferations of atypical spindled cells with enlarged hyperchromatic nuclei (Fig. 13B). As in the larger MPNSTs, brisk mitotic activity (Fig. 13B, arrows) was readily identified in the microtumors. The identity of these lesions was confirmed by their immunoreactivity for S100β (Fig. 13C) and nestin (Fig 13D). We conclude that MPNSTs in P_0GGFβ3;*Trp53*$^{+/-}$ mice, like those in *cis-Nf1*$^{+/-}$;*Trp53*$^{+/-}$ mice (26), arise *de novo* rather than from a neurofibroma precursor.

We noted that the cellularity and number of mitotic figures was lower in the microtumors than in the larger MPNSTs found in these animals. To determine whether the microtumors were lower grade MPNSTs and to clearly distinguish them from neurofibromas, we quantified expression of the Ki67 proliferation marker and performed TUNEL labeling in three major MPNSTs and three microtumors derived from P_0-GGFβ3;*Trp53*$^{+/-}$ mice, three neurofibromas identified in outbred P_0-GGFβ3 mice, three hyperplastic trigeminal ganglia from 1 month old P_0-GGFβ3 mice and three normal trigeminal ganglia from 1 month old C57BL/6J wild-type mice. We found extensive nuclear Ki67 immunoreactivity in the major MPNSTs (Fig. 14A), with Ki67 labeling indices that averaged 46.4% (Fig. 14E). Ki67 labeling was also readily detected in the microtumors (Fig. 14B). However, Ki67 labeling in the microtumors (average labeling index, 12.3%) was significantly less than we observed in the major MPNSTs (Fig. 14E). On the other hand, Ki67 labeling in the microtumors was significantly higher than that in neurofibromas, hyperplastic transgenic ganglia or wild-type ganglia; indeed, Ki67 labeling was difficult to detect in these three latter types of specimens. TUNEL labeling was also readily detected in the major MPNSTs (Fig. 14C) and microtumors (Fig. 14D), demonstrating the occurrence of a baseline level of apoptosis. However, TUNEL labeling was not significantly increased in the major MPNSTs relative to the microtumors (Fig. 14F; 8.2% versus 7%).

If the microtumors are the progenitor lesions that develop into the major MPNSTs, we would anticipate that the microtumors would tend to be lower grade malignancies while the major MPNSTs would predominantly be higher grade lesions. To evaluate this possibility, we graded all of the microtumors and the major MPNSTs identified in our P_0-GGFβ3;*Trp53*$^{+/-}$ cohort using WHO criteria for

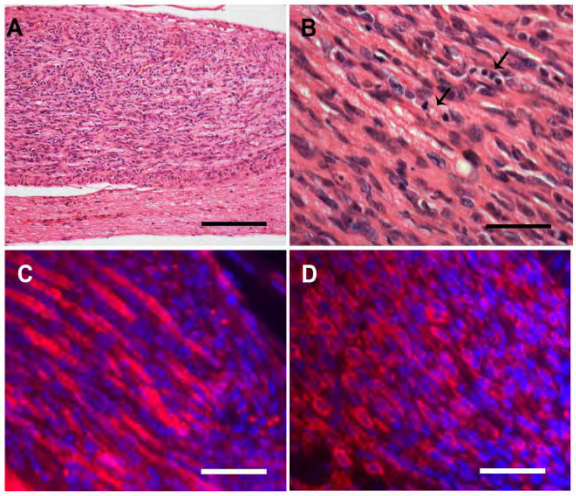

Fig. 13 MPNSTs occurring in P_0-GGFβ3;*Trp53*$^{+/-}$ mice develop within peripheral nervous system ganglia. **A:** A markedly hypercellular microtumor developing within the trigeminal ganglion of a P_0-GGFβ3;*Trp53*$^{+/-}$ mouse. Scale bar, 100μm. **B:** Higher power view of the tumor shown in A. Note the increased nuclear size and atypia within this lesion and the frequent occurrence of mitotic figures (arrows). **C:** Immunostain demonstrating S100β immunoreactivity in the microtumor cells and Schwann cells associated with entrapped axons in the lesion. **D:** Like the major MPNSTs, the microtumors also show nestin immunoreactivity. Scale bars in B-D, 50μm.

the grading of human MPNSTs (1). As shown in Table 5, 59% (10/17) of the microtumors met diagnostic criteria for WHO grade II MPNSTs, while 41% (7/17) of the microtumors were classified as WHO grade III MPNSTs. None of the microtumors had the features of grade IV MPNSTs. In contrast, the majority of the major MPNSTs were high grade tumors, with 38% (8/21) of the major MPNSTs having the diagnostic features seen in human WHO grade IV MPNSTs, 52% (11/21) of these tumors being WHO grade III MPNSTs and only 10% (2/21) of the major MPNSTs (2/21) meeting WHO grade II diagnostic criteria. Considered collectively, the observations noted above suggest that MPNSTs initially develop *de novo* as low grade intraganglionic malignancies in P_0-GGFβ3;*Trp53*$^{+/-}$ mice. As these low grade MPNSTs expand, they presumably accumulate additional genomic abnormalities, resulting in their progression to become high grade (WHO grade III-IV) MPNSTs. Thus, P_0-GGFβ3;*Trp53*$^{+/-}$ mice represent a new model useful for studying the evolution of genomic changes in MPNSTs as they progress from low grade (WHO grade II) to high grade (WHO grade III-IV) tumors.

In addition to the work described above, we have made extensive progress in our genomic analyses of P_0-GGFβ3 MPNSTs. This work, which is as yet unpublished (as it is still ongoing), addresses all of the tasks in Specific Aim 1:

Subtask 1: Isolate RNA and genomic DNA from cultures suitable for analysis (months 1-12). We have isolated high quality total cellular RNA (which is to be used for RNA-Seq) and genomic DNA (which is to be used for exome sequencing and array CGH) from P_0-GGFβ3 40 MPNSTs. We have also isolated high quality genomic DNA and total cellular RNA from a panel of 19 human MPNST cell lines and a series of surgically resected human MPNSTs. These human specimens will form the validation set that will be used to establish that abnormalities identified in P_0-GGFβ3 MPNSTs are relevant to the pathogenesis of their human counterparts and thus are useful therapeutic targets.

Subtask 2: Perform aCGH experiments with genomic DNA isolated from the cultures (months 3-24). **In addition to the array CGH experiments that we have already published in our first manuscript, we have completed the aCGH experiments on the remainder of our 40 MPNSTs (i.e., an additional 29 tumors).** In addition, one of the reviewers for our second manuscript requested that we perform array CGH on some of the MPNSTs from our P_0-GGFβ3;*Trp53*$^{+/-}$ mouse model so that we can demonstrate that the changes occurring in these tumors are equivalent to those seen in P_0-GGFβ3 MPNSTs. We thought that this was a splendid idea as it will further validate the utility of this model for studying the genomic abnormalities involved in MPNST progression. Identifying these changes is critically important as it has important implications for the treatment of these tumors. Speaking as a pathologist who deals clinically with the difficult issue of grading MPNSTs and distinguishing low grade MPNSTs from atypical neurofibromas (a very common problem; in fact, I have such a case sitting on my desk right now), identifying genomic abnormalities associated with different stages in the evolution of this tumor series would also greatly improve our diagnostic accuracy.

Subtask 3: Perform RNA-Seq experiments with RNA isolated from the cultures (months 3-24). **We have completed RNA-Seq on our first two tumors and have completed our initial analysis of these results. We have also isolated the total cellular RNA from all 40 P_0-GGFβ3 MPNSTs for performing RNA-Seq.** To ensure technical consistency, these specimens will all be transported to

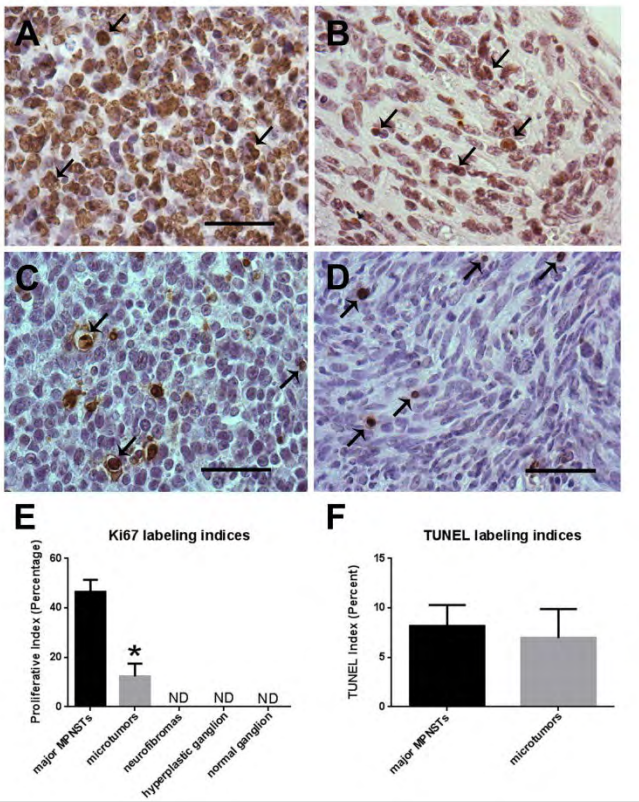

Fig. 14 Ki67 labeling indices in the microtumors occurring in P_0-GGFβ3;*Trp53*$^{+/-}$ mice are higher than seen in neurofibromas and non-neoplastic ganglia but lower than is seen in the larger tumors present in these animals. **A, B:** Major MPNST (**A**) and micro-MPNST (**B**) stained for the proliferative marker Ki67 shown side-by-side for comparison. **C, D:** DNA fragmentation in major MPNSTs **(C)** and microtumors **(D)**, as labeled via TUNEL. **E:** Quantification of Ki67 labeling in major MPNSTs, micro-MPNSTs (microtumors), neurofibromas, neoplastic ganglia, and non-neoplastic ganglia demonstrates a significant difference between major MPNSTs and micro-MPNSTs (p<0.0001; n=3 animals per specimen type). **F:** Quantification of TUNEL labeling in major MPNSTs and micro-MPNSTs shows no significant difference in labeling indices. Scale bars in A-D, 50μm.

MUSC and sequenced using the Illumina HiSeq 2500 instrument housed in the Center for Genomic Medicine at MUSC.

Subtask 4: Perform exome sequencing experiments with genomic DNA isolated from the cultures (months 3-24). **We have finished sequencing the whole exomes of all of our planned 40 tumors.** This data is very high quality (typically representing 60-fold or greater coverage of the entire exome), with greater than 99% of the reads mapping to the reference mouse genome. To identify any single nucleotide polymorphisms (SNPs) that might not be represented in the dbSNP database, we also assembled a pool of genomic DNA isolated from 12 C57BL/6J mice and a second pool derived from 12 SJL/J mice; these correspond to the genetic background of our A colony mice (C57BL/6J x SJL/J) and our B colony mice (C57BL/6J). We have finished whole exome sequencing on these specimens as well. SNPs identified in these pools that are not present in the dbSNP database are being used as a second filter for distinguishing germline and somatic mutations in our P_0-GGFβ3 MPNSTs.

Subtask 5: Perform bioinformatic analyses of results from experiments described in a-d (months 3-36). As noted above, we have completed our initial analyses of the two RNA-Seq datasets. We have also completed our initial analyses of 12 of the exome sequences. During the course of these analyses, we made a key observation regarding the accuracy of identifying novel nonsynonymous SNPs. We identified many such SNPs in both the transcriptome and exomes of these tumors. However, identifying these changes as genuine mutations rather than sequencing errors was frequently more difficult in the transcriptome than in the exome. This is because transcripts that are lower abundance will, by definition, have a lower-fold coverage in the RNA-Seq dataset. Consequently, we would encounter situations where (even in the high quality datasets we have generated) there might be only 2-3 reads across a region and one of those reads had a SNP. In this circumstance, it could not be clearly determined whether these changes represented a true mutation. In contrast, in our exome datasets the variability in depth of coverage was much lower and it was much more obvious when a SNP represented a true mutation rather than a sequencing error (i.e., the same change was present in multiple reads, which is highly unlikely for a sequencing error). Given this, we prioritized the sequencing of our tumor exomes for the purpose of identifying point mutations, frameshift mutations and small indels.

KEY RESEARCH ACCOMPLISHMENTS

- We have identified a number of candidate mutations potentially promoting MPNST pathogenesis that can now be evaluated as therapeutic targets in these tumors.

REPORTABLE OUTCOMES

MANUSCRIPTS, ABSTRACTS and PRESENTATIONS

Manuscripts

1) Kazmi SJ, Byer SJ, Eckert JM, Turk AN, Huijbregts RPH, Brossier NM, Grizzle WE, Mikhail FM, Roth KA and **Carroll SL**. Transgenic mice overexpressing neuregulin-1 model neurofibroma-malignant peripheral nerve sheath tumor progression and implicate specific chromosomal copy number variations in tumorigenesis. *The American Journal of Pathology* 2013; 182(3): 646-677. PMID: 23321323 PMCID: PMC3586689 ***Highlighted Article****:* see *The American Journal of Pathology* 2013; 182(3): 611
2) Brosius SN, Turn AN, Byer SJ, Brossier NM, Kohli L, Whitmire A, Mikhail FM, Roth KA and **Carroll SL**. Neuregulin-1 overexpression and *Trp53* haploinsufficiency cooperatively promote *de novo* malignant peripheral nerve sheath tumor pathogenesis. *Acta Neuropathologica* 2014; 127: 573-591. PMID: 24243507 PMCID: PMC3999224

Abstracts

1) Warram JM, Turk A, Martin A, **Carroll S** and Zinn KR. FDG-PET for detection of spontaneous malignant peripheral nerve sheath tumors in a transgenic animal model. *Proceeding of World Imaging Congress* 2012; Abstract nr P114.
2) Brosius SN, Turk AN, Byer SJ, Brossier NM, Kohli L, Roth KA and **Carroll SL**. Neuregulin-1 overexpression and p53 haploinsufficiency cooperatively promote *de novo* MPNST pathogenesis. *FASEB Journal* 2013; 27: 380.2.
3) Brosius SN, Roth KA and **Carroll SL**. Combinatorial treatment of malignant peripheral nerve sheath tumors with tyrosine kinase inhibitors hinders proliferation and survival. *FASEB Journal* 2013; 27: 1088.4.
4) **Carroll SL**, Byer SJ, Cai Z, Chi CL, Huang CY, Gafni ES, Murphy CJ, Ravvaz K, Du R, Turk AJ, Gannon MA, Korf BR, Roth KA, Almeida JS and Tonellato PJ. Identification of novel gene fusions in malignant peripheral nerve sheath tumors using paired-end transcriptome sequencing. *Journal of Neuropathology and Experimental Neurology* 2013; 72(6): 575.
5) Brosius SN, Byer SJ, Moon A, Roth KA, and **Carroll SL.** Aberrantly expressed erbB4 promotes malignant peripheral nerve sheath tumor pathogenesis. *Journal of Neuropathology and Neurology* 2014; 73(6): 616.

Presentations

1) Brosius SN, Turk AN, Byer SJ, Brossier NM, Kohli L, Roth KA and **Carroll SL**. Neuregulin-1 overexpression and p53 haploinsufficiency cooperatively promote *de novo* MPNST pathogenesis. Platform Presentation, “Stem Cell Biology and Molecular Profiling in Malignancies” Minisymposium, American Society for Investigative Pathology/Experimental Biology 2013 Meeting (Boston, MA), April 20, 2013.
2) **Carroll SL.** Invited Speaker, Medical University of South Carolina Department of Pathology (Charleston, SC), “From Humans to Mice and Back Again: Translational Cancer Genomics in Mouse Models of Peripheral Nervous System Neoplasia”, May 22, 2013
3) **Carroll SL.** Invited Speaker, University of Texas Medical Branch Department of Pathology (Galveston, TX), “From Humans to Mice and Back Again: Translational Cancer Genomics in Mouse Models of Peripheral Nervous System Neoplasia”, October 23, 2013
4) **Carroll SL**, Byer SJ, Cai Z, Chi CL, Huang CY, Gafni ES, Murphy CJ, Ravvaz K, Du R, Turk AJ, Gannon MA, Korf BR, Roth KA, Almeida JS and Tonellato PJ. Identification of novel gene fusions in malignant peripheral nerve sheath tumors using paired-end transcriptome sequencing. American Association of Neuropathologists 2013 Annual Meeting (Charleston, SC).

LICENSES APPLIED FOR AND/OR ISSUED

None.

DEGREES OBTAINED THAT ARE SUPPORTED BY THIS AWARD

Stephanie N. Brosius, B.A. (Washington University in St. Louis)

UAB Medical Scientist Training Program (MD-PhD) Student, Carroll Lab Trainee (2011-2014)
Admitted to candidacy for the Ph.D. degree, 22 November 2012
Recipient, Histochemical Society 2012 Trainee Travel Award
Recipient, Histochemical Society-Sponsored 2013 Trainee Travel Award
2013 Histochemical Society Ralph D. Lillie Award for Outstanding Abstract
Recipient, NINDS Predoctoral Fellowship Award (1 F31 NS081824-01; 07/01/13-06/30/16)
Second Place, Data Blitz graduate student oral presentation competition, 2013 UAB Neuroscience Retreat
Best Poster, 2013 Medical Student Research Day
Recipient, 2014 UAB Samuel B. Barker Award for Excellence in Graduate Studies at the Doctoral Level
Ph.D. Thesis: "Determining the role of neuregulin-1 and its erbB receptors in the pathogenesis of malignant peripheral nerve sheath tumors" successfully defended May 30, 2014
Currently: Medical Student, University of Alabama at Birmingham (Birmingham, AL).

DEVELOPMENT OF CELL LINES, TISSUE OR SERUM REPOSITORIES

1) Established early passage cultures from 90 P_0-GGFβ3 MPNSTs
2) Established early passage cultures from 12 P_0-GGFβ3;*Trp53*$^{+/-}$ MPNSTs

DATABASES AND ANIMAL MODELS

1) P_0-GGFβ3;*Trp53*$^{+/-}$ mouse, which models MPNST progression from WHO grade II to WHO grade IV

FUNDING APPLIED FOR BASED ON WORK SUPPORTED BY THIS AWARD

Project #:	1 F31 NS081824-01	Dates: 07/01/13-06/30/16	
Source:	NIH/NINDS	Direct Costs/Yr: $32,879	
Title:	*Evaluating the Role of NRG-1 Receptors in MPNST Tumorigenesis*		
PI:	Brosius, S.N. (UAB M.D.-Ph.D. student)		
Mentor:	Carroll, S.L.	% Effort:	0%

Note: This grant has been funded.

EMPLOYMENT OR RESEARCH OPPORTUNITIES APPLIED FOR AND/OR RECEIVED BASED ON EXPERIENCE/TRAINING SUPPORTED BY THIS AWARD

None.

CONCLUSIONS

We have shown that the vast majority of transgenic mice overexpressing the NRG1 isoform GGFβ3 in Schwann cells develop numerous neurofibromas and smaller numbers of MPNSTs which potentially arise from pre-existing neurofibromas. These observations, considered together with our finding that the same molecular abnormalities occurring in human neurofibromas and MPNSTs are present in P_0-GGFβ3 MPNSTs, argue that P_0-GGFβ3 mice appropriately model the process of neurofibroma-MPNST progression seen in human NF1 patients. A number of previous studies have commented on the fact that chromosomal gains and losses are highly variable in human MPNSTs and that tumor suppressors such as p53 are not uniformly mutated in these neoplasms. These observations suggest that there may be more than one pathway leading to MPNST pathogenesis. As neurofibroma and MPNST formation in P_0-GGFβ3 mice results from growth factor overexpression rather than from ablation of specific tumor suppressor genes, tumorigenesis in these animals, unlike in previous knockout models, is not necessarily dependent upon the mutation of a restricted collection of tumor suppressors; this suggestion is consistent with our observation that key tumor suppressor mutations (e.g., p53) and focal CNVs were variably present in P_0-GGFβ3 MPNSTs. Consequently, P_0-GGFβ3 mice represent a novel model system that can be used to identify alternative pathways mediating neurofibroma-MPNST progression.

We have also found that tumorigenesis is suppressed in transgenic mice overexpressing NRG1 in Schwann cells, which suggests that a modifier gene or genes capable of suppressing neurofibroma pathogenesis is present in the C57BL/6J genetic background. Genetic complementation experiments

in which inbred P_0-GGFβ3 mice were crossed to *Nf1*$^{+/-}$ or *Trp53*$^{+/-}$ mice showed that, while tumorigenesis was absent in the P_0-GGFβ3;*Nf1*$^{+/-}$ animals, P_0-GGFβ3;*Trp53*$^{+/-}$ mice developed MPNSTs. Further, the MPNSTs seen in P_0-GGFβ3;*Trp53*$^{+/-}$ mice developed *de novo* rather than from neurofibromas as in seen in the parent P_0-GGFβ3 line. These observations clarify the role that NRG1 plays in PNS neoplasia as they indicate that NRG1 promotes tumorigenesis primarily via its effects on the signaling cascades that are affected by neurofibromin loss. In keeping with our earlier suggestion that neurofibromas and MPNSTs originate intraganglionically, we have also now shown that the MPNSTs in P_0-GGFβ3;*Trp53*$^{+/-}$ mice originate from microtumors that develop within PNS ganglia. Unexpectedly, P_0-GGFβ3;*Trp53*$^{+/-}$ mice have proven to be a new model of PNS neoplasia that is potentially useful for identifying key mutations mediating the progression of low grade MPNSTs to higher grade tumors. Consequently, partnering genomic analyses of the various MPNST grades occurring in P_0-GGFβ3;*Trp53*$^{+/-}$ mice with similar analyses of the neurofibromas and MPNSTs that develop in P_0-GGFβ3 mice will give us a global understanding of the evolution of neurofibromas and MPNSTs and will identify important new therapeutic targets in these tumors.

Our current ongoing studies are directed towards expanding our array CGH experiments to include a larger cohort of P_0-GGFβ3 neurofibromas and MPNSTs and examining these neoplasms with RNA-Seq and exome sequencing so that more subtle mutations promoting peripheral nervous system tumorigenesis can be identified and considered as potential therapeutic targets.

REFERENCES
APPENDICES

References

1. Scheithauer BWL, D.N.:Hunter, S.;Woodruff, J.M.;Antonescu, C.R. Malignant peripheral nerve sheath tumour (MPNST). In: Louis DNO, H.;Wiestler,O.D.;Cavenee,W.K., editor. WHO Classification of Tumours of the Central Nervous System. Lyon: IARC; 2007. p. 160-2.

2. Huijbregts RP, Roth KA, Schmidt RE, Carroll SL. Hypertrophic neuropathies and malignant peripheral nerve sheath tumors in transgenic mice overexpressing glial growth factor beta3 in myelinating Schwann cells. J Neurosci. 2003;23:7269-80.

3. Woodruff JMK, H.P.; Louis,D.N.; Scheithauer,B.W. Malignant peripheral nerve sheath tumour (MPNST). In: Kleihues PC, W.K., editor. Pathology and Genetics of Tumours of the Nervous System. First ed. Lyon: IARC Press; 2000. p. 172-4.

4. Basu TN, Gutmann DH, Fletcher JA, Glover TW, Collins FS, Downward J. Aberrant regulation of ras proteins in malignant tumour cells from type 1 neurofibromatosis patients. Nature. 1992;356:713-5.

5. DeClue JE, Papageorge AG, Fletcher JA, Diehl SR, Ratner N, Vass WC, et al. Abnormal regulation of mammalian p21ras contributes to malignant tumor growth in von Recklinghausen (type 1) neurofibromatosis. Cell. 1992;69:265-73.

6. Guha A, Lau N, Huvar I, Gutmann D, Provias J, Pawson T, et al. Ras-GTP levels are elevated in human NF1 peripheral nerve tumors. Oncogene. 1996;12:507-13.

7. Berner JM, Sorlie T, Mertens F, Henriksen J, Saeter G, Mandahl N, et al. Chromosome band 9p21 is frequently altered in malignant peripheral nerve sheath tumors: studies of CDKN2A and other genes of the pRB pathway. Genes Chromosomes Cancer. 1999;26:151-60.

8. Kourea HP, Orlow I, Scheithauer BW, Cordon-Cardo C, Woodruff JM. Deletions of the INK4A gene occur in malignant peripheral nerve sheath tumors but not in neurofibromas. Am J Pathol. 1999;155:1855-60.

9. Nielsen GP, Stemmer-Rachamimov AO, Ino Y, Moller MB, Rosenberg AE, Louis DN. Malignant transformation of neurofibromas in neurofibromatosis 1 is associated with CDKN2A/p16 inactivation. Am J Pathol. 1999;155:1879-84.

10. Birindelli S, Perrone F, Oggionni M, Lavarino C, Pasini B, Vergani B, et al. Rb and TP53 pathway alterations in sporadic and NF1-related malignant peripheral nerve sheath tumors. Lab Invest. 2001;81:833-44.

11. Perry A, Kunz SN, Fuller CE, Banerjee R, Marley EF, Liapis H, et al. Differential NF1, p16, and EGFR patterns by interphase cytogenetics (FISH) in malignant peripheral nerve sheath

tumor (MPNST) and morphologically similar spindle cell neoplasms. J Neuropathol Exp Neurol. 2002;61:702-9.
12. Perrone F, Tabano S, Colombo F, Dagrada G, Birindelli S, Gronchi A, et al. p15INK4b, p14ARF, and p16INK4a inactivation in sporadic and neurofibromatosis type 1-related malignant peripheral nerve sheath tumors. Clin Cancer Res. 2003;9:4132-8.
13. Agesen TH, Florenes VA, Molenaar WM, Lind GE, Berner JM, Plaat BE, et al. Expression patterns of cell cycle components in sporadic and neurofibromatosis type 1-related malignant peripheral nerve sheath tumors. J Neuropathol Exp Neurol. 2005;64:74-81.
14. Sabah M, Cummins R, Leader M, Kay E. Loss of p16 (INK4A) expression is associated with allelic imbalance/loss of heterozygosity of chromosome 9p21 in microdissected malignant peripheral nerve sheath tumors. Appl Immunohistochem Mol Morphol. 2006;14:97-102.
15. Endo M, Kobayashi C, Setsu N, Takahashi Y, Kohashi K, Yamamoto H, et al. Prognostic significance of p14ARF, p15INK4b and p16INK4a inactivation in malignant peripheral nerve sheath tumors. Clin Cancer Res. 2011;17:3771-82.
16. Kourea HP, Cordon-Cardo C, Dudas M, Leung D, Woodruff JM. Expression of p27(kip) and other cell cycle regulators in malignant peripheral nerve sheath tumors and neurofibromas: the emerging role of p27(kip) in malignant transformation of neurofibromas. Am J Pathol. 1999;155:1885-91.
17. Zhou H, Coffin CM, Perkins SL, Tripp SR, Liew M, Viskochil DH. Malignant peripheral nerve sheath tumor: a comparison of grade, immunophenotype, and cell cycle/growth activation marker expression in sporadic and neurofibromatosis 1-related lesions. Am J Surg Pathol. 2003;27:1337-45.
18. Pugh TJ, Weeraratne SD, Archer TC, Pomeranz Krummel DA, Auclair D, Bochicchio J, et al. Medulloblastoma exome sequencing uncovers subtype-specific somatic mutations. Nature. 2012.
19. Jones DT, Jager N, Kool M, Zichner T, Hutter B, Sultan M, et al. Dissecting the genomic complexity underlying medulloblastoma. Nature. 2012.
20. Northcott PA, Shih DJ, Peacock J, Garzia L, Sorana Morrissy A, Zichner T, et al. Subgroup-specific structural variation across 1,000 medulloblastoma genomes. Nature. 2012.
21. Rozenblatt-Rosen O, Deo RC, Padi M, Adelmant G, Calderwood MA, Rolland T, et al. Interpreting cancer genomes using systematic host network perturbations by tumour virus proteins. Nature. 2012;487:491-5.
22. Prasad R, Leshkowitz D, Gu Y, Alder H, Nakamura T, Saito H, et al. Leucine-zipper dimerization motif encoded by the AF17 gene fused to ALL-1 (MLL) in acute leukemia. Proc Natl Acad Sci U S A. 1994;91:8107-11.
23. Chin L, Hahn WC, Getz G, Meyerson M. Making sense of cancer genomic data. Genes Dev. 2011;25:534-55.
24. Boyden LM, Lewis JM, Barbee SD, Bas A, Girardi M, Hayday AC, et al. Skint1, the prototype of a newly identified immunoglobulin superfamily gene cluster, positively selects epidermal gammadelta T cells. NatGenet. 2008;40:656-62.
25. Kazmi SJ, Byer SJ, Eckert JM, Turk AN, Huijbregts RP, Brossier NM, et al. Transgenic mice overexpressing neuregulin-1 model neurofibroma-malignant peripheral nerve sheath tumor progression and implicate specific chromosomal copy number variations in tumorigenesis. Am J Pathol. 2013;182:646-67.
26. Vogel KS, Klesse LJ, Velasco-Miguel S, Meyers K, Rushing EJ, Parada LF. Mouse tumor model for neurofibromatosis type 1. Science. 1999;286:2176-9.
27. Cichowski K, Shih TS, Schmitt E, Santiago S, Reilly K, McLaughlin ME, et al. Mouse models of tumor development in neurofibromatosis type 1. Science. 1999;286:2172-6.
28. Shimada S, Tsuzuki T, Kuroda M, Nagasaka T, Hara K, Takahashi E, et al. Nestin expression as a new marker in malignant peripheral nerve sheath tumors. Pathol Int. 2007;57:60-7.
29. Olsen SH, Thomas DG, Lucas DR. Cluster analysis of immunohistochemical profiles in synovial sarcoma, malignant peripheral nerve sheath tumor, and Ewing sarcoma. Mod Pathol. 2006;19:659-68.

Table 1. Whole Chromosome/Large Region Gains and Losses in P_0-GGFβ3 MPNSTs

Chromosome	Tumor Cultures
Chromosome 1	
Whole chromosome gain	B86, B91, B96
Chromosome 3	
Whole chromosome gain	A18, B76
Chromosome 4	
Whole chromosome loss	A202
Chromosome 6	
Whole chromosome gain	A18, B76, B86, B91
Chromosome 7	
Whole chromosome gain	A18, A292
Chromosome 8	
Whole chromosome loss	A202
Whole chromosome gain	B76
Chromosome 9	
Whole chromosome loss	A202, A390
Chromosome 10	
Whole chromosome gain	A382
Loss (3,051,721-50,790,081)	B76
Chromosome 11	
Whole chromosome gain	A18, A202, A231Tr, A292, A382, A390, A394, B76, B86, B91, B96
Chromosome 12	
Whole chromosome gain	A231Tr, A202
Loss (86,353,623-120,684,848)	A382
Chromosome 13	
Whole chromosome loss	A202
Chromosome 14	
Loss (12,738,652-125,076,290)	A18
Loss (8,760,452-125,076,290)	A202
Gain (8,794,768-125,076,290)	B76
Chromosome 15	
Whole chromosome gain	A18, A231Tr, B76, B91
Chromosome 16	
Whole chromosome loss	A202, A390
Chromosome 17	
Whole chromosome gain	A18, A292, A394, B76, B91
Chromosome 18	
Whole chromosome loss	A390
Chromosome 19	
Whole chromosome loss	A202, A390
Whole chromosome gain	A382, B86, B96
Gain (10,320,214-61,216,212)	B91
Chromosome X	
Whole chromosome gain	A18, A202, A390, A394, B91

Table 2. Genes within Small/Minimal Critical Regions of Gain or Loss in P_0-GGFβ3 MPNSTs

Minimal Critical Region	Cell Lines	Genes
Chromosome 1		
18,123,973-20,989,757 (Gain)	A18	Crisp4, Defb18, Defb49, Defb41, Gm15386, Tcfap2d, Tcfap2b, **Pkhd1**, Mir206, **Il17a**, Il17f, AK205147, Mcm3, Paqr8, Efhc1
172,530,936-172,637,996 (Loss)	A390	Olfm12b, Atf6
173,444,742-173,494,144 (Loss)	A292, B96, B91, B86, B76	BC145376, Itln1, Cd244
Chromosome 2		
27,740,854-27,893,558 (Gain)	A202	Col15a1, BC152372
85,976,236-86,076,234 (Gain)	A231Tr	Olfr1040, Olfr1042, Olfr1043, Olfr1044, Olfr52, Olfr1045, Olfr1046, Olfr1047, Olfr1048
86,061,726-86,087,429 (Loss)	A202, A18	Olfr1047, Olfr1048
118,994,902-119,055,137 (Loss)	A18	Gchfr, Dnajc17, Gm14137, Zfyve19, Ppp1r14d
163,824,466-163,964,059 (Loss)	A18	Ywhab, Pabpc1l, 1810053B01Rik, Tomm34, **Stk4**
165,860,752-165,971,779 (Loss)	A18	**Ncoa3**, **Sulf2**
Chromosome 3		
8,919,417-9,605,520 (Gain)	A202	Mrps28, **Tpd52**, AK016002, Zbtb10, C030034L19Rik, Zfp704
Chromosome 4		
47,961,806-52,868,964 (Loss)	A390	AK133250, **Nr4a3**, Stx17, Erp44, Invs, Tex10, 5730528L13Rik, Tmeff1, Murc, E130309F12Rik, Acnat2, Acnat1, AK018513, Baat, Mrp150, **Aldob**, Zfp189, Rnf20, Ppp3r2, 2810432L12Rik, Grin3a, Cylc2, S60135, S60130, AK012547, Smc2, 4930547C10Rik, Olfr275
62,162,092-62,182,694 (Gain)	A231Tr, A202, A18, A390	Hdhd3, **Alad**
88,168,201-88,829,428 (Loss)	A382	Ifnb1, Gm12597, Ifna14, Ifna9, Ifna12, C87499, Ifna13, Gm13280, Ifna2, Ifnab, Klh19, Gm13271, Gm13285, Gm13276, Ifnz, Gm13275, Gm13287, Ifna7, Ifna11, Ifna6, Ifna5, Ifna4, Ifna1, Ifn3, Mir31, AK144962, Gm12603, Mtap
88,934,158-89,039,587 (Loss)	A231Tr, B96, B91, B86, A382, A292	**Cdkn2a**, AK148321, **Cdkn2b**
98,831,785-99,056,334 (Gain)	A202	Atg4c
111,745,189-112,130,291 (Gain)	A231Tr, B96, B91, B86, B76, A394, A382, A292, A202, A390	Skint4, Skint3, Skint9
Chromosome 5		
110,540,802-111,792,099 (Gain)	A202	Zfp605, **Chfr**, AK053084, Golga3, Ankle2, Pgam5, Pxmp2, Pole, P2rx2, Gm1679, Fbrsl1, 2410025L10Rik, AK088579, AK041600, Galnt9, Ddx51, **Ep400**, Noc4l, AK044789, Pus1, Ulk1, Hscb, **Chek2**, Ttc28, Mir701, Pitpnb, AK039279
124,704,754-124,838,557 (Loss)	A18	Mphosph9, 281006K23Rik, **Cdk2ap1**, **Sbno1**
Chromosome 7		
12,807,582-14,904,447 (Gain)	A18	Vmn1r81, Vmn1r82, Vmn1r83, Vmn1r84, Zfp551, Zfp606, 290092C05Rik, Vmn2r53, Vmn2r54, Vmn2r55, Vmn2r56, Zscan18, Zfp329, Zfp110, Zfp128, **Zscan22**, Rp25, Zfp324, 2310014L17Rik, Zfp446, Zbtb45, Slc27a5, Trim28, Chmp2a, Ube2m, Mzf1, Vmn1r86, Vmn1r85, Vmn1r87, Vmn1r88, Vmn1r89, 6330408A02Rik, AK132923, Lig1, Pla2g4c, Cabp5, Bsph1, 9230107M04Rik, Bsph2, Sult2a5, Sult2a2, Sult2a1, Sult2a4, Sult2a3, Sult2a6, EG629219
16,685,001-17,087,560 (Loss)	A18	**Napa**, Kptn, Slc8a2, Meis3, mKIAA0134, Dhx34, Gpr77, C5ar1, Prr24, Ccdc9, **Bbc3**, Sae1,

		Zc3h4, Tmem160, Npas1, Grlf1
19,998,996-20,191,762 (Gain)	B76	Ckm, AK020867, mKIAA1860, **Mark4**, Exoc312, Bloc1s3, Trappc6a, Nkpd1, Lrrc68, AK195979, Gemin7, Zfp296, Sfrs16, Clasrp, Rel
54,644,122-54,885,354 (Gain)	B86	Mrgpra2a, Mrgpra2b, Mrgpra3
123,174,938-123,176,223 (Loss)	A292, A382	Sox6
Chromosome 9		
103,906,930-103,968,229 (Gain)	A18	Nphp3, Uba5, Acad11
Chromosome 10		
80,128,600-80,381,401 (Loss)	A394, B91	Mknk2, Mnk2, Mobkl2a, Izumo4, Ap3d1, Dot1l, Plekhj1, Sf3a2, Amh, Jsrp1, Oaz1, Mir1982, AK087942, Lingo3, Lsm7, 3110056O03Rik, Spp12b, Tmprss9, Timm13, Lmnb2
80,993,669-83,063,521 (Gain)	B76	**Gna11**, Aes, Tle2, Tle6, Sirt6, BC025920, Ankrd24, Gm10778, BC064812, Zfp781, AK136722, BC062115, **Zfp873**, AU041133, B230315N10Rik, Mif1, Gm1553, 1190007I07Rik, Tdg, Glt8d2, Hcfc2, Nfyb, AK006461, Txnrd1, Eid3, Chst11, Slc41a2, D10Wsu102e, Aldh1l2, Appl
93,173,564-93,303,322 (Gain)	A202	Ntn4, AK145310, DQ556351, Usp44
125,404,179-127,428,204 (Gain)	A18	Lrig3, AK005576, Xrcc6bp1, AK087024, Ctdsp2, Mir26a-2, Mir546, Avil, Tsfm, Mettl1, Cyp27b1, **Cdk4**, Tspan31, March9, **Agap2**, Os9, B4galnt1, Slc26a10, Arhgef25, **Dtx3**, Deltex3, AK077682, Pip4k2c, Kif5a, Dctn2, Mbd6, **Ddit3**, **Mars**, **Arhgap9**, **Gli1**, **Inhbe**, Inhbc, R3hdm2, Stac3, Ndufa4l2, Shmt2, Nxph4, Lrp1, Stat6, Nab2, BC029853, AK005897, Tmem194, Myo1a, Tac2, Zbtb39, Gpr182, Rdh1, Rdh9, Rdh16, Rdh18-ps, BC089597, Rdh7, Sdr9c7, Hsd17
Chromosome 12		
37,823,207-37,970,476 (Loss)	A292	Meox2, Tmem195
115,837,534-117,190,767 (Gain)	A202, A18	Antibody parts, X73024, AB345949
Chromosome 14		
21,275,133-22,200,898 (Loss)	A18	Anxa7, Zmynd17, Ppp3cb, 1810062O18Rik, Usp54, Myoz1, Synpo2l, Sec24c, AK018074, AK204442, 6230400D17Rik, 2310021P13Rik, Kiaa0913, Ndst2, Camk2g, AK039280, Plau, **Vcl**, Ap3m1, Adk
53,008,490-54,874,949 (Gain)	B86	Olfr1511, Olfr1510, **TCRA**, Olfr1509, Olfr1508, Olfr1507, Gm10886, AJ311366, X98059, Z22845, Gm13948, Gm10905, X56719, D16605, Gm13960, Gm10895, Gm13980, ENSMUSG000000836, Vdelta6.4, GM16979, GM13907, AK138453, X02930, Gm10902, AK038197, EG547424, M21205, X56722, X02969, Gm16460, Gm16979, Gm13907, U07879, Gm16980, Gm13980, AK038197, EG547424, Gm17002, Gm13953, Gm13948, Gm16452, M34214 and multiple TCR-alpha genes
69,877,095-69,987,156 (Gain)	A390, B76, B86, B91, B96	Slc25a37, D930020E02Rik, AK046510, Entpd4, AK086749, BC086315
Chromosome 15		
3,228,882-4,824,497 (Gain)	A390	Sepp1, Ccdc152, **Ghr**, Fbxo4, AW549877, AK041537, BC037032, Oxct1, AK028088, Plcxd3, C6
60,562,187-62,065,471 (Gain)	A202, A390	Fam84b, 9930014A18Rik, DQ715236, AK015045, A1bg, EU234017, AK163289, AK132958, **Myc**, **Pvt1**, H2afy2

71,284,106-72,565,945 (Gain)	A390	Fam135b, Col22a1, Kcnk9, Trappc9
Chromosome 16		
43,620,829-43,773,291 (Gain)	B76	Zbtb20, AK038731, Mir568, Tigit, Drd3
Chromosome 17		
30,714,112-31,047,626 (Loss)	A231Tr, A202, B86, A390, A382	Glo1, Dnahc8, AK018977, Glp1r
79,124,627-79,148,417 (Gain)	B91	**Strn**
Chromosome 19		
32,866,825-32,944,421 (Loss)	A202	**Pten**, B430203M17Rik
Chromosome X		
7,276,714-7,415,340 (Gain)	A394	Gpkow, Wdr45, Praf2, Ccdc120, Mir684-1, Tcfe3, Gripap1, Kcnd1
34,183,857-34,755,807 (Gain)	B76	Akap17b, Slc25a43, Slc25a5, C330007P06Rik, Ube2a, Nkrf, **Sept6**, Ankrd58, Rp139, Snora69, Upf3b, Nkap, Akap14, Ndufa1, Rnf113a1, Gm9, Rhox1
39,447,121-40,770,156 (Loss)	A292	**Xiap**, Stag2, Xlp, Sh2d1a, Odz1, Ten-m1
153,911,519-153,991,073 (Gain)	A202	Sms, Mbtps2

Bolded and underlined genes: Cancer driver genes represented in the Atlas of Genetics and Cytogenetics in Oncology and Haematology, CANgenes, CIS and/or Sanger Cancer Gene Census databases.

Table 3. Functions of Candidate Driver Genes in Small Regions of Unbalanced Gain and Loss

Gene	***Function***
Pkhd1 (polycystic kidney and hepatic disease 1)	Cilium assembly, centrosome duplication
Il17a (interleukin 17A)	Inflammatory response
Stk4 (serine/threonine kinase 4)	Hippo signaling cascade
Ncoa3 (nuclear receptor coactivator 3)	Ligand-dependent transcription factor
Sulf2 (sulfatase 2)	Extracellular sulfatase
Tpd52 (tumor protein D52)	Promotes proliferation, survival and metastasis; regulates lysosomal trafficking
Nr4a3 (nuclear receptor subfamily 4, group A, member 3)	Ligand-dependent transcription factor
Aldob (aldolase B, fructose-biphosphate)	Glycolysis
Alad (aminolevulinate, delta-, dehydratase)	Heme biosynthesis
Cdkn2a (cyclin-dependent kinase inhibitor 2A)	Cell cycle arrest
Cdkn2b (cyclin-dependent kinase inhibitor 2B)	Cell cycle arrest
Chfr (checkpoint with forkhead and ring finger domains	Mitotic checkpoint protein, maintains chromosome integrity
Ep400 (E1A binding protein p400, mDomino)	ATP-dependent chromatin-remodeling protein
Chek2 (checkpoint kinase 2, Rad53)	DNA damage checkpoint control
Cdk2ap1 (CDK2-associated protein 1)	Negative regulator of Cdk2 function
Sbno1 (strawberry notch homolog 1)	Unknown
Zscan22 (zinc finger and SCAN domain containing 22	Gli-Kruppel family transcription factor
Napa (N-ethylmaleimide sensitive fusion protein attachment protein alpha)	Trans-Golgi vesicle trafficking
Bbc3 (Bcl binding component 3; PUMA)	p53-regulated inducer of apoptosis
Mark4 (MAP/microtubule affinity-regulating kinase 4)	Serine-threonine kinase
Gna11 (guanine nucleotide binding protein, alpha 11)	G-protein coupled receptor signaling mediator
Zfp873 (zinc finger protein 873)	Unknown
Cdk4 (cyclin-dependent kinase 4)	Cell cycle progression
Agap2 (ArfGAP with GTPase domain, ankyrin repeat and PH domain 2)	Regulator of ARF activity
Dtx3 (deltex 3 homolog)	Notch signaling pathway
Ddit3 (DNA damage-inducible transcript 3; GADD153, CHOP10)	Promotes cell cycle arrest, macroautophagy
Mars (methionine-tRNA synthetase)	Charges Met-tRNA with methionine
Arhgap9 (Rho GTPase activating protein 9)	Inactivates Rho signaling
Gli1 (GLI-Kruppel family member GLI1)	Transcription factor that promotes proliferation, Hedgehog signaling pathway
Inhbe (inhibin beta E, activin E)	Growth factor
Vcl (vinculin)	Adherens junction component, modulates focal adhesion
TCRA (T cell receptor genes)	Antigen recognition
Ghr (growth hormone receptor)	Growth hormone receptor
Myc (myelocytomatosis oncogene)	Nuclear phosphoprotein regulating cell cycle progression, apoptosis and transformation
Pvt1 (plasmacytoma variant translocation 1)	Encodes multiple microRNAs
Strn (striatin, calmodulin binding protein)	Cytoplasmic signaling molecule, inhibits proliferation
Pten (phosphatase and tensin homolog)	Inhibits PI3 kinase activity
Sept6 (septin 6)	Cytoskeleton, regulates motility
Xiap (X-linked inhibitor of apoptosis)	Inhibits apoptosis

Table 4. Distribution of MPNSTs in P_0-GGFβ3;*Trp53*$^{+/-}$ Mice

Location	**Percentage**
Mice with tumors at any location	95%
Trigeminal tumors	58%
Spinal dorsal nerve root tumors	68%
Sciatic nerve tumors	11%
Multiple tumors	53%

Table 5. WHO grades of major and micro tumors developing in P_0-GGFβ3;*Trp53*$^{+/-}$ mice

Mouse #	Tumor Location	Sex	Major or Micro	WHO Grade
H6	DRG	Male	Major	IV
H9	Trigeminal ganglion	Female	Major	III
H17	Trigeminal ganglion	Male	Major	II
H19	Sciatic	Female	Major	IV
	Trigeminal ganglion	Female	Micro	II
	DRG	Female	Micro	II
H24	Sciatic	Female	Major	III
	DRG	Female	Micro	III
	DRG	Female	Major	IV
H32	DRG	Male	Major	IV
H46	DRG	Female	Major	IV
	DRG	Female	Micro	III
	DRG	Female	Micro	II
H72	DRG	Female	Micro	II
	Trigeminal ganglion	Female	Major	III
H73	Trigeminal ganglion	Female	Major	III
H76	Trigeminal ganglion	Male	Major	II
	DRG	Male	Micro	II
	DRG	Male	Major	IV
H77	Trigeminal ganglion	Male	Major	III
H81	Trigeminal ganglion	Male	Major	III
	DRG	Male	Major	IV
	DRG	Male	Major	III
	DRG	Male	Major	III
H83	DRG	Male	Major	IV
	Trigeminal ganglion	Male	Micro	II
	DRG	Male	Micro	III
H88	DRG	Male	Micro	II
	DRG	Male	Micro	II
	Trigeminal ganglion	Male	Micro	II
	Trigeminal ganglion	Male	Micro	III
H89	Trigeminal ganglion	Male	Micro	III
H90	DRG	Female	Micro	II
H99	Trigeminal ganglion	Female	Micro	III
	DRG	Female	Major	III
	DRG	Female	Micro	III
	DRG	Female	Major	III
H103	Trigeminal ganglion	Female	Major	III